Influence of Switching Dynamics on the Solvent Extraction Process of Polymer Droplets

by

Romain Billet

A thesis submitted in partial fulfillment of the requirements for the degree of

Master of Science

in

Materials Engineering

Department of Chemical and Materials Engineering
University of Alberta

Abstract

Switchable hydrophilicity solvents (SHSs) are solvents defined by their ability to switch from their hydrophobic form to a hydrophilic form when put in contact with an acidic trigger such as CO_2. As a consequence, SHSs qualify as promising alternatives to volatile organic compounds during the industrial solvent extraction processes, as greener and inexpensive methods can be applied to separate and recover SHSs. Furthermore, because of their less volatile nature, SHSs are less flammable and so increase the safety of a larger-scale extraction process. However, the use of SHSs also comes with challenges related to the long switching times and high residual solvent left in extraction products.

In the first part of this work, we study the dynamics and in-drop phase separation during the dissolution process of a sessile binary drop composed of the SHS N,N-Dimethylcyclohexylamine (DMCHA) and polystyrene, triggered by an acid in the surrounding aqueous environment. From 70 different experimental conditions, we found a scaling relationship between the drop dissolution time and initial volume with an overall scaling coefficient ~ 0.53. We quantitatively assessed and found a shorter dissolution time related with a decrease in pH of the aqueous phase or an increase in initial polymer concentration in the drop. Our experimental results provide a microscopic view of the SHS dissolution process from polymer drops. Examining the internal state of the drop during the dissolution revealed an in-drop phase separation behavior, resulting in a porous morphology of the final polymer particle.

In the second part of this work, we study the effects from switching conditions on the solvent residue during the formation of polystyrene latexes induced by emulsion

extraction. The extraction of DMCHA from emulsion droplets containing polystyrene was triggered by addition of an acid in the surrounding aqueous phase. We found a constant level of the solvent residue in the final polystyrene particles regardless of the trigger addition rate and trigger solution concentration. However, a decrease in the solvent residue was achieved at higher fractions of the organic dispersed phase in the emulsion or at lower extraction temperature. The solvent residue may be attributed to the formation of water-oil-water emulsion during the extraction process.

Overall, the work presented in this thesis highlights the phase separation behavior and the link between residual solvent and trapped water. The dynamics of drop dissolution and mechanism for the presence of residual solvent reported in this work may help design SHS extraction processes for particle formation with effective approaches for reducing the residual solvent left after dissolution.

Preface

This thesis is an original work written by me, Romain Billet. The chapters of this work are constituted by the following modified manuscripts in which I am the first author:

1. **Billet Romain**, Binglin Zeng, James Lockhart, Michael Gattrell, Hongying Zhao, Xuehua Zhang. 'Dissolution Dynamics of a Binary Switchable Hydrophilicty Solvent - Polymer Drop into an Acidic Aqueous Phase'. Soft Matter, 2022. I was the main author of this work and was responsible for experiments, data analysis, writing and revisions of the manuscript. Binglin Zeng helped with the experimental, provided matlab tools for data analysis, and gave valuable comments on improving the figures, introduction and discussion parts. James Lockhart, Mike Gattrell, and Hongying Zhao were industrial collaborators who helped lead my research throughout the months and provided feedback on the full manuscript. Xuehua Zhang was the supervisor for this work, and was involved at every steps of the research, data collection and analysis, as well as editing the manuscript. Chapters 1 and 2 were respectively written using modified portions of the introduction and experimental section. This work's results and discussion sections are found in Chapter 3.

2. **Billet Romain**, Binglin Zeng, Hongyan Wu, James Lockhart, Mike Gattrell, Hongying Zhao, and Xuehua Zhang. "Effects of Switching Conditions on Switchable Solvent Residue in Polystyrene Microparticles from Emulsion Extraction". Manuscript under preparation. I was the primary author of this work and was

in charge of the experiments, data analysis and writing. Binglin Zeng assisted in the editing of the manuscript as well as the design of the figures. Hongyan Wu contributed to the Raman detection experimental setup and provided criticism on the manuscript. James Lockhart, Mike Gattrell, and Hongying Zhao were industrial partners that assisted in the direction of my research over the course of several months and offered feedback on the final publication. Xuehua Zhang acted as the project's supervisor and was involved in all aspects of the research, including data collection and analysis, as well as manuscript editing. Chapters 1 and 2 were respectively written using modified portions of the introduction and experimental section. This work's results and discussion sections are found in Chapter 4.

Acknowledgements

My supervisor, Dr. Xuehua Zhang, deserves a special mention, so please accept my sincere gratitude. I appreciate all of the time and assistance that you gave me during this thesis work, as well as your patience and support. You taught me a lot, and this experience helped me develop into a better person. I was able to advance and develop as a scientist because she constantly encouraged me to be the best version of myself. I will never forget this experience, and I know that what I learnt in the Soft Matter & Interfaces group will be crucial to my professional success in the long run.

In addition, I want to express my gratitude to Hongying Zhao, James Lockhart, Mike Gattrell and Hassan Hamza without whom I would not have been able to finish this project. I appreciate the guidance, positivity, and wise counsel you provided me during our monthly meetings.

I appreciate all the aid I received from Dr. Binglin Zeng, Hongyan Wu, and Qiuyun Lu as well as their insightful remarks and conversation.

I'm also appreciative of the friendship and support I've received from each and every member of the Soft Matter & Interfaces group, past and present. It was a delight to work with this group, and I hope to work with another one in the future that is equally enjoyable.

I acknwoledge Mitacs Accelerate Program, BC Research,the Canada Foundation for Innovation (CFI), the Natural Science and Engineering Research Council of Canada (NSERC) and Alberta-innovates for funding support. I am also grateful for the technical assistance from IOSI Labs at the Faculty of Engineering.

Table of Contents

List of Tables

List of Figures

List of Symbols

D	Baseline diameter
Da	Damköhler number
H	Height of the drop
K_a	Acid dissociation constant
M	Drop mass
R	Drop radius
R_0	Initial drop radius
Ra	Rayleigh number
V	Drop volume
V_0	Initial drop volume
Δc	Difference of concentration between the drop surface and far away from the drop
α	Prefactor
β_c	Solutal expansion coefficient
γ	Scaling coefficient
κ	Diffusion coefficient of the drop material into the surrounding liquid
ν	Kinematic viscosity of the surrounding liquid
ρ	Drop material density
ρ_b	Surrounding liquid density
ρ_{DMCHA}	Density of pure DMCHA
ρ_{PS}	Density of pure PS
ρ_{mix}	Mixture density

τ	Drop lifetime
θ	Contact angle
θ_0	Initial contact angle
c_s	Solubility of DMCHA
$f(\theta)$	First geometrical factor
g	Acceleration of gravity
$g(\theta)$	Second geometrical factor
k_r	Reaction rate constant of the switching off reaction
k_s	Reaction rate constant of the switching reaction
$logK_{OW}$	Logarithm of the octanol-water partition coeffient
pH	Potential of hydrogen
x_{DMCHA}	Mass fraction of DMCHA
x_{PS}	Mass fraction of PS

Abbreviations

CA-mode Constant contact angle mode.

CR-mode Constant radius mode.

DLLME Dispersive liquid-liquid phase microextraction.

DMBA N,N-Dimethylbenzylamine.

DMCHA N,N-Dimethylcyclohexylamine.

DPA Dipropylamine.

FA Formic acid.

FBRM Focused beam reflectance measurement.

LLE Liquid-liquid phase extraction.

LLME Liquid-liquid phase microextraction.

LOD Limit of detection.

LOQ Limit of quantification.

PBMA Poly(butyl methacrylate).

PS Polystyrene.

SDS Sodium dodecyl sulfate.

SEM Scanning electron microscopy.

SHS Switchable hydrophilicity solvent.

SHS-LLME Switchable hydrophilicity solvent liquid-liquid phase microextraction.

TEA Triethylamine.

VOC Volatile organic compound.

Chapter 1

Introduction

.

1.1 Background

1.1.1 Switchable hydrophilicity solvents

Switchable Hydrophilicity Solvents (SHSs) are solvents insoluble in water in their neutral form [1, 2]. However, as shown in fig. 1.1(a), when contacted with a trigger, such as CO_2, the SHS switches from its neutral insoluble form to a protonated, soluble form in water. This switching process is also reversible, and SHS can be "switched" back to their hydrophobic form by, for example, removing CO_2 by flushing with N_2.

The general mechanism driving the switching process of SHSs is an acid (trigger) base (SHS) reaction:

$$\mathrm{SHS_{org}} + \mathrm{H^+_{aq}} \rightleftharpoons \mathrm{SHSH^+_{aq}}$$

Some common triggers that have been used to switch SHSs include carbonic acid in water H_2CO_3 by CO_2 bubbling, addition of dry ice [3–5] or Na_2CO_3 [6, 7], and acids such as HCl [8–10], H_2SO_4 and H_3PO_4 [11].

Studies examined many chemicals reported to be SHSs and identified chemical and physical features typical of SHSs [12–14]. It has been discovered that the compounds' SHS nature is influenced by their basicity, as shown by their pKa, as well as their

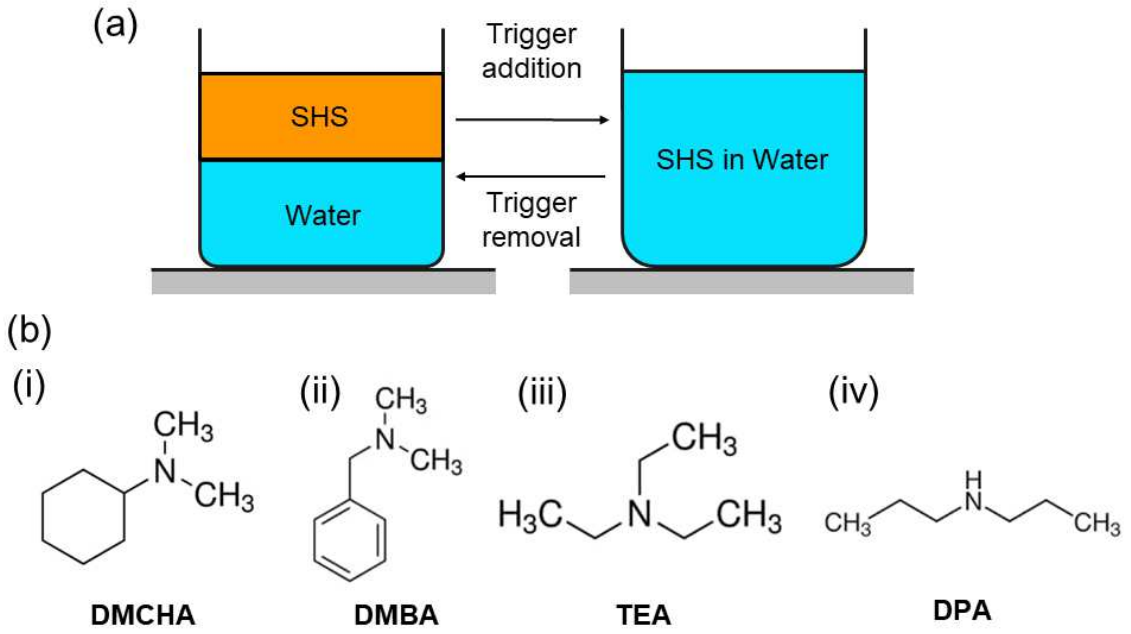

Figure 1.1: (a) Sketch of the working principle of SHSs. In their neutral form, SHSs are insoluble with water, but when a trigger is added, SHSs are able to become soluble in water. This process is reversible by removal of the trigger from the mixture. (b) Molecular structures of commonly used SHSs. (i) N,N-Dimethylcyclohexylamine (DMCHA), (ii) N,N-Dimethylbenzylamine (DMBA), (iii) Triethylamine (TEA), (iv) Dipropylamine (DPA).

partitioning characteristics. It has been suggested that favourable conditions for SHSs include a pKa value over 9.5 and an octanol-water partition coefficient $logK_{OW}$ between 1.2 and 2.5, which is defined as the log of the ratio of the concentration of a chemical molecule between the two immiscible phases of octanol and water.

Most of the SHSs described in applications are amines, with the majority being tertiary or secondary amines. Fig. 1.1(b) shows the molecular structure of commonly used SHSs. In particular, SHSs (i-iii) are tertiary amines, while SHS (iv) represent a secondary amine. However, recent works has expanded the solvents to diamines with improved phase behavior [15] or amine-free SHS [16].

Solvent removal is one of the most common processes in the chemical industry. Being able to remove and recover the solvent from a system is of the utmost importance and can be done by evaporation induced by heating and/or vacuum. A

common way to make such solvent removal and recovery easier is to use low boiling point Volatile Organic Compounds (VOCs). However, these solvents are also usually hazardous pollutants known for their toxicity and smog-forming properties [17, 18] These VOCs are also typically highly flammable, requiring special considerations in the design and operation of the solvent recovery processes. To respect the principles of green-chemistry, the search for an alternative is necessary [19, 20]. In this perspective, SHSs present an economically viable and green alternative to VOCs due to the simplicity to "switch on" and "off" the hydrophobicity of the solvent with high recoverability coming from the "switching off" process.

1.1.2 Applications of SHSs

SHSs for Extraction

Applications of SHSs regularly include extractions. Extractions are methods developed to separate a compound of interest from a matrix. In liquid-liquid phase extractions (LLE), the compound of interest is separated by partitioning between two immiscible phase. The phase of higher solubility therefore becomes the extractant phase that can be separated from the second immiscible liquid phase. A solvent removal step is then necessary to recover the compound of interest by removing the extractant solvent. For SHSs, this solvent removal step can be achieved by mixing the SHS with water and switching the SHSs to its hydrophilic form. The SHS is therefore removed in the aqueous phase, allowing the recovery of the compound of interest. The SHS can then be recovered and recycled from the aqueous phase by removing the trigger, and can therefore be reused for a new extraction.

A typical example of extraction using a SHS has been demonstrated in the separation of bitumen from oil sands [21]. Fig. 1.2(a) shows the working principle of the extraction of bitumen using DMCHA as the SHS and extractant phase. By first dissolving the bitumen in oil sands, DMCHA enables its separation from the sand matrix. The DMCHA can then be removed out of the sand and incorporated into

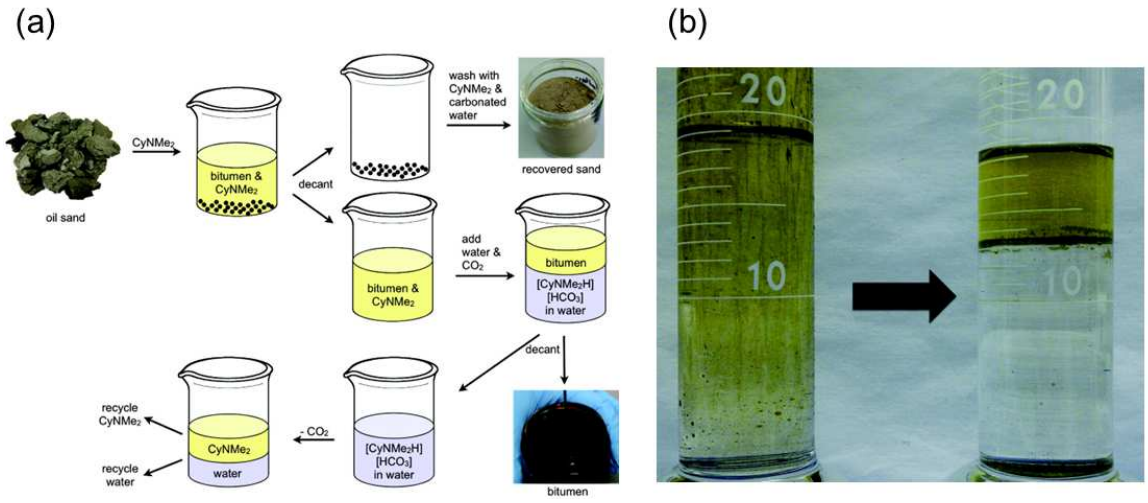

Figure 1.2: (a) Sketch representing the extraction of bitumen from oil sand using DMCHA as the SHS and extractant phase. (b) Image of the monophasic mixture of water and DMCHA on the left, and biphasic mixture after removing CO_2 from the aqueous phase on the right. Figure adapted from ref. [21].

a water phase. In order to dissolve DMCHA in water and recover the extracted bitumen, CO_2 is added as the trigger. After separation of the bitumen from the aqueous layer, DMCHA can also be recycled and utilised in another extraction cycle by eliminating CO_2 from the aqueous phase with a purge of N_2, as shown in fig. 1.2(b).

Other applications of SHSs for extraction have been demonstrated in soybean oil extraction [22, 23], biofuel extraction from microalgae [24–28], phenols extraction [29, 30] or plastics [2, 31] and multi-layer packaging recycling [32–34],

Switchable Hydrophilicity Liquid-Liquid Microextraction (SHS-LLME) for Analytical Chemistry

Dispersive Liquid-Liquid Microextration (DLLME) is a method of extraction requiring the extraction phase to be dispersed inside of the liquid containing analytes to extract [35, 36]. Using a disperser, the extraction phase exists as emulsion droplets of high surface to volume ratio inside the other liquid phase. This allows a fast mass transfer from the continuous phase to the extraction phase of the analytes, and therefore short extraction times. The emulsion can then be centrifuged to recover the

extractant phase that can be coupled with analytical chemistry detection or quantification methods.

SHSs have previously been used as the extractant phase in liquid-liquid microextraction to extract substances from aqueous matrices, resulting in the SHS-LLME subset of microextractions [37, 38]. For this type of microextraction, a trigger is used to first dissolve the SHS in analyte-containing water. By switching off the SHS, an emulsion of SHS in water is formed, resulting in rapid extraction of the analytes. Using SHSs provides several advantages over other traditional extractants. In addition to being greener solvents, SHSs do not need any dispersing solvent to create an emulsion. Due to their hydrophobicity in their neutral form and lack of a dispersing solvent, SHSs also function as a highly unstable emulsion that can be recovered without centrifugation. SHS-LLME has been used to detect metal ions in environmental samples [5, 39–42], drugs in human urine [9–11, 43, 44] or pesticides [45–47]

SHSs for latexes formation

Latexes are defined as stable dispersion of polymer particles in water. They are used in numerous applications, such as gloves manufacture [48], paints [49] or coatings [50]. Latexes can be found naturally, such as the well-known rubber extracted in latex form from the *Hevea Brasiliensis* [51] or prepared artificially.

Methods to prepare artificial latexes include radical emulsion polymerization [52–54], and direct emulsification. In the latter, a polymer solution is emulsified in water, and the solvent is then removed by evaporation induced by heating [55–58]. Direct emulsification present the advantage to avoid traces of monomer or initiator in the final product. However, to simplify the solvent removal step, VOCs are used to dissolve polymers.

SHS removal has been shown to work effectively for different latex formation via emulsion switching of N,N-dicyclohexylmethylamine, including poly(butyl methacrylate) (PBMA), natural rubber, poly(methyl methacrylate), poly(ethyl methacrylate)

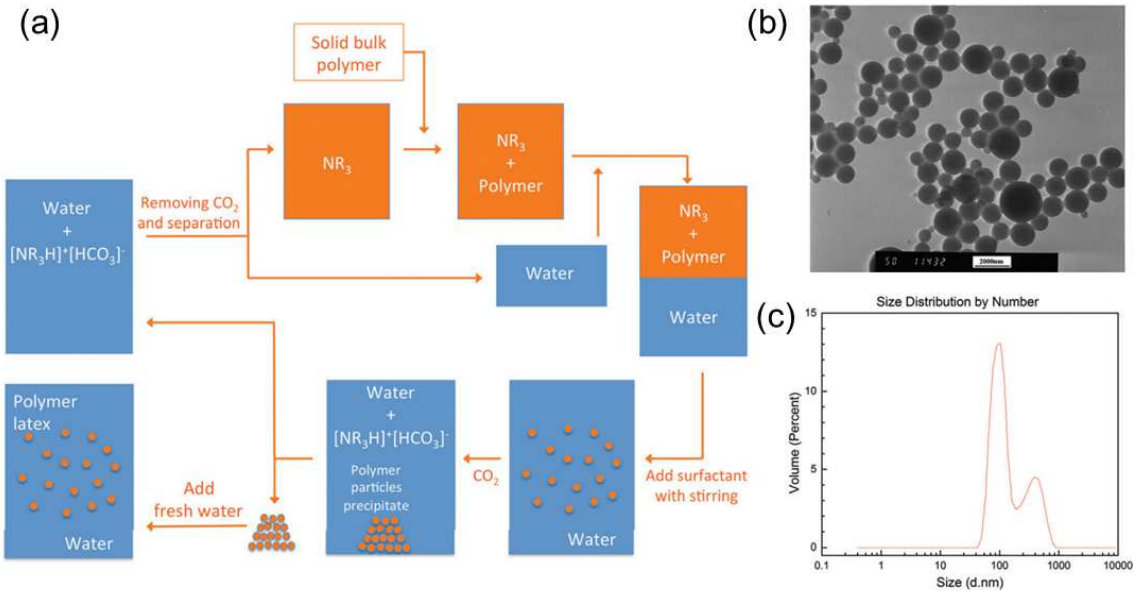

Figure 1.3: (a) Sketch of the latex formation method using SHS. A SHS/polymer mixture is emulsified in water, and the SHS is removed by addition of the trigger to recover polymer a latex. (b) TEM image of the PBMA latex recovered via emulsion extraction. (c) Corresponding size distribution of the latex. Figure adapted from ref. [59]

and polystyrene (PS) latexes [59]. Fig. 1.3(a) shows the process of latex formation by using SHSs. A mixture of polymer and SHS is first prepared and emulsified, creating droplets of SHS/polymer in water that are stabilized by a surfactant. The SHS is then made to switch and dissolve in the water, only leaving polymer particles in the water. Due to the high ionic strength of the medium after switching and formation of the SHS salt, the polymer particles aggregate, allowing for the recovered polymer to be separated from the aqueous phase. As shown in 1.3(b), the polymer particles can be dispersed again in a fresh aqueous phase to create a latex. Fig. 1.3(c) shows the size distribution of the PBMA latex formed by this method. The size of the particles was measured to be between 100 nm and 2 μm over all the latexes produced. The SHS-contaminated aqueous phase, on the other hand, can be switched off in order to recover the SHS, which can then be used for the next cycle.

1.1.3 Droplet dissolution

Droplet dissolution dynamics

How fast a droplet can dissolve in an under saturated environment has been the subject of numerous studies and models. The simplest model used to describe the dissolution process relies on the diffusion mechanism. The diffusion-driven, or Epstein-Plesset [60] model was first established for a bulk gas bubble inside of an under saturated liquid, and later confirmed to be experimentally applicable for bulk oil droplets in an under saturated liquid [61]. Solving the diffusion equation for the spherical drop, it is possible to find a relation between the time and the radius of the drop:

$$R = R_0 * \sqrt{1 - 2\frac{\kappa \Delta c}{\rho R_0^2} t} \tag{1.1}$$

With R the droplet radius, R_0 the initial radius of the droplet, ρ the droplet material density, κ the diffusion coefficient of the droplet material inside of the surrounding liquid and Δc, the difference between the concentration of the droplet material at the droplet surface and far away from the droplet, and t the time since the beginning of the dissolution. This results in the following scaling law between the droplet initial volume V_0 and drop lifetime τ, with A a constant:

$$\tau = A * \frac{\rho}{\kappa \Delta c} V_0^{\frac{2}{3}} \tag{1.2}$$

We can see that a scaling coefficient with $\frac{2}{3}$ is expected from the diffusion-dominated dissolution. The Epstein-Plesset model only describes the dissolution of a bulk droplet, or "free" droplet in a liquid environment following a dissolution mechanism, and therefore assumes a complete spherical symmetry. This model can also be modified to fit to the sessile droplet geometry [62, 63]. In the sessile drop dissolution model, the droplet is assumed to have a spherical-cap shape and follows a diffusive mechanism for mass transport.

$$\frac{dM}{dt} = \frac{\pi}{2} D\kappa\Delta c f(\theta) \tag{1.3}$$

With M the total mass of the droplet, D the baseline diameter of the droplet and $f(\theta)$ the following function of the contact angle θ of the droplet:

$$f(\theta) = \frac{sin(\theta)}{1 + cos(\theta)} + 4\int_0^\infty \frac{1 + cosh(2\theta\xi)}{sinh(2\pi\xi)} tanh[(\pi - \theta)\xi]\,\mathrm{d}\xi \tag{1.4}$$

The function f adds the description of the droplet geometry to the diffusion problem. By introducing this geometrical factor, the dynamic of the baseline diameter becomes coupled with the change in contact angle.

Different modes of sessile droplet dissolution have been seen in various studies. As shown in Fig. 1.4(a), pinning effects can fix the contact line of the droplet and force the drop to dissolve with a constant baseline diameter (Constant Radius mode, CR-mode). On the opposite side, as shown inf Fig. 1.4(b) , the contact angle can remain constant while the drop baseline diameter shrinks (Constant Angle mode, CA-mode) [63–66].

It has also been observed that during dissolution, both the CR and CA modes could be combined to form intermediary modes. Fig. 1.4(c) describes the stick-slide mode, which corresponds to a succession of CR and CA modes. Fig. 1.4(d) represents the stick-jump to a CR mode until a sudden depinning of the contact line leading to a decrease in the baseline radius and increase in the contact angle [63, 67].

Depending on the dissolution mode of the sessile drop, equation 1.3 can be simplified, and in some cases, solved analytically [63]. For the CR and CA dissolution mode respectively, equation 1.3 leads to equation 1.5 and equation 1.6

$$\frac{d\theta}{dt} = -\frac{4\kappa\Delta c}{\rho D^2}(1 + cos(\theta))^2 f(\theta) \tag{1.5}$$

$$D\frac{dD}{dt} = \frac{4\kappa\Delta c}{\rho}\frac{f(\theta)}{3g(\theta)} \tag{1.6}$$

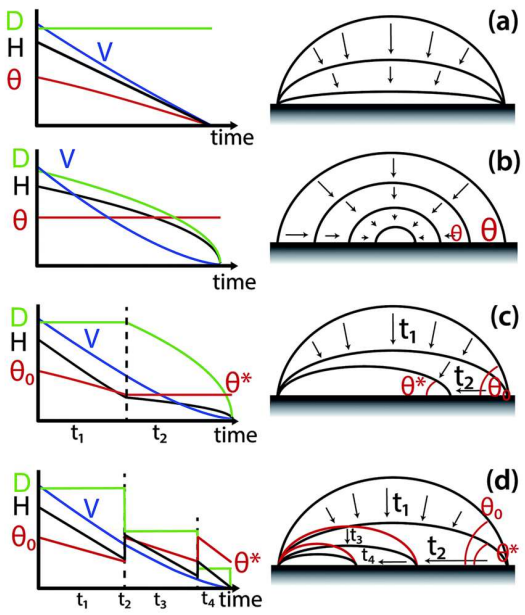

Figure 1.4: Sketch of the different dissolution modes for a sessile drop, and plot of the corresponding baseline diameter D, height of the drop H, contact angle θ, and droplet volume V. (a) CR-Mode, (b) CA-mode, (c) Stick-slide mode, (d) Stick-jump mode. Figure adapted from ref. [63]

With g the following function of the contact angle :

$$g(\theta) = \frac{cos^3(\theta) - 3cos(\theta) + 2}{3sin^3(\theta)} \tag{1.7}$$

For the CA-mode, equation 1.6 can be solved analytically, and similarly to the Epstein-Plesset model, a scaling law can be extracted:

$$\tau = A'(\theta) * \frac{\rho}{\kappa \Delta c} V_0^{\frac{2}{3}} \tag{1.8}$$

With $A'(\theta)$ another geometrical constant depending on the constant contact angle θ. Once again, the lifetime of the drop follows a power scaling law with the initial volume V_0, with a scaling coefficient of $\frac{2}{3}$

These previous models consider one mechanism for the mass transport during the dissolution which is the diffusion of the droplet liquid in an under saturated environment. However, other mechanisms can also be added to explain the observed

dissolution. One of them describes how natural convection influences mass movement out of the droplet by enhancing the natural flow coming from the droplet [68]. The mechanism driving the convection dissolution model is that the dissolved droplet liquid alters the density of the liquid layer around the droplet surface. As a consequence of this density change, the boundary layer is subjected to buoyancy forces, creating convection cells that bring fresh liquid to the surface. These convection cells enhance the mass transport and lead to a new scaling law:

$$\tau = A''(\theta) * (\frac{\nu\rho^4}{g\beta_c\Delta c^5\kappa^3})^{\frac{1}{4}} V_0^{\frac{5}{12}} \tag{1.9}$$

With $A''(\theta)$ a new geometrical constant depending on the contact angle, ν the kinematic viscosity of the surrounding liquid and g the acceleration of gravity. β_c is the solutal expansion coefficient defined by $\beta_c = \frac{1}{\rho_b}\frac{\partial\rho}{\partial c}$, with ρ_b the pure surrounding liquid density and $\frac{\partial\rho}{\partial c}$ the change in density of the surrounding liquid with a concentration c of the droplet liquid is dissolved in it.

Dissolution of multicomponent droplets

The dissolution process of multicomponent drops, as opposed to pure liquid drops, has been found to exhibit complex dynamics depending on the nature of the drop components. In a multicomponent drop, preferential dissolution of some components has been shown to influence the dynamics of the dissolution [69, 70]. The change in composition during the dissolution process has also been shown to trigger phase segregation [70] or microdroplet nucleation [71].

When droplets with soluble components and one immiscible phase dissolve, the immiscible phase is left behind, which causes particles to form. The final particles obtained from such dissolution processes may lead to variety of structures as shown in fig. 1.5, useful to design particles for specific applications. Colloidal droplets composed of insoluble particles inside of the drop phase have been shown to lead to self-assembly and toroidal structures [72, 73], while snowballs of colloidal graphene

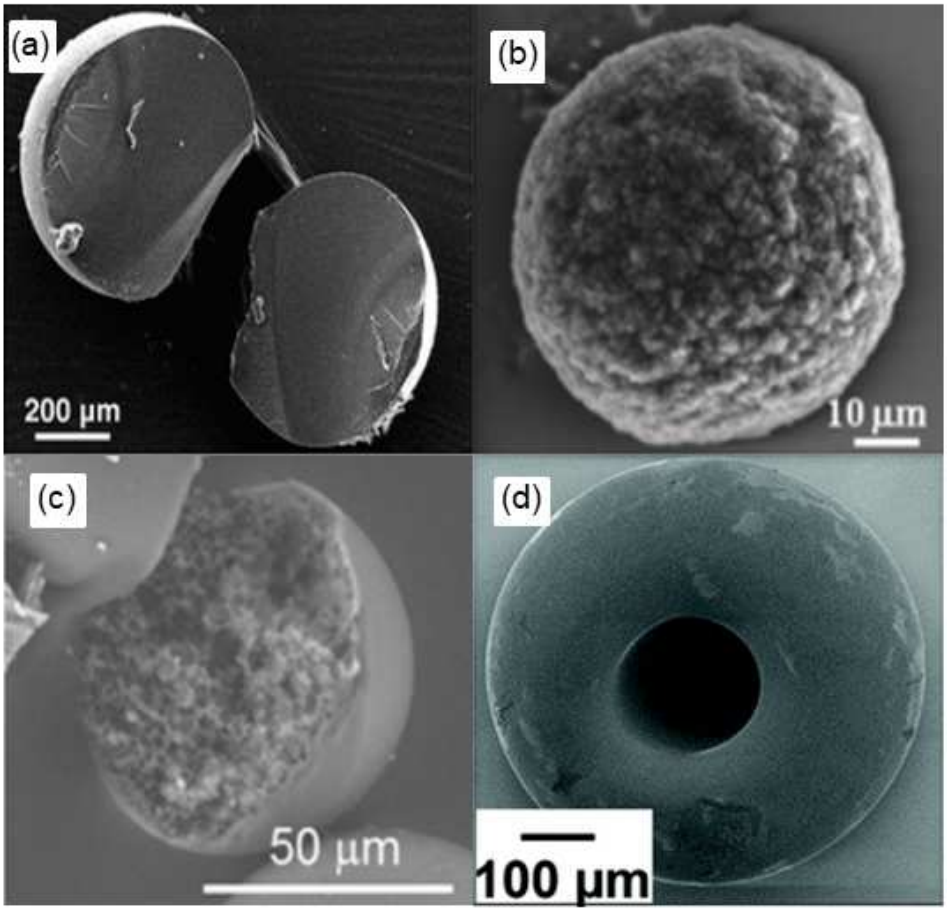

Figure 1.5: Different particle structures emerging from dissolution of droplets containing one component insoluble in the dissolution liquid. SEM images of the particles resulting from the dissolution of (a) silk fibroin solution droplets, (b) graphene oxide dispersion droplets, (c) polymer solution droplets and (d) SiO_2 particles suspension droplets. Figure adapted from ref. [72, 74, 78, 79]

oxide may develop from drop dissolution [74, 75]. Dissolution of polymer solution drops has been shown to lead to formation of porous particles [76–78], while silk solution drops were able to form transparent particles with regular microstructures [79].

1.2 Motivation for this project

The dissolution of SHS/polymer droplets, induced by switching of the SHS, is of particular interest for applications such as latexes formation [59]. However, the switching

SHS and corresponding solvent extraction process has previously been shown to be time consuming, in some cases reaching hours [12]. It is therefore important to understand what conditions may possibly shorten the switching-extraction time and minimize residual solvent in a cost-effective manner. In the extraction process assisted by CO_2-switching SHS, two steps may play a role: (1) the slow mass transfer of CO_2 gas into the aqueous phase, followed by the chemical reactions of dissociation and hydrolysis of CO_2 to HCO_3^-, CO_3^{2-} and H^+, and (2) the liquid phase reaction (switching) of neutral SHS (hydrophobic form) and dissolution of switched SHS (hydrophilic form) into the aqueous solution. In previous works [80, 81], the acceleration of the switching-extraction dynamics was studied using a microfluidic device. The improved specific interfacial area between the aqueous phase and CO_2 gas accelerated the extraction process inside the microfluidic device. However, to the best of our knowledge, there is no quantitative understanding on the SHS dissolution dynamics of the reaction-induced mass transfer of the SHS, and in-particular inside a liquid drop and its impact on the final morphology of the polymer particles post solvent extraction.

Furthermore, a recurrent issue hindering the development of commercial applications of SHS extraction processes has been the high residual solvent found in the product recovered after extraction. The amount of residual solvent may depend on the type of SHS and extracted compound, but also on extraction conditions such as water content, temperature or stirring conditions. In polystyrene recycling, 8 wt% of residual DMCHA was found in the polystyrene phase [2]. Lower, but still existing residual solvent was found during multilayer packaging recycling, with 1 - 4 wt% of DMCHA in the low density polyethylene phase [32] and during PBMA latex formation, with around 2.5 wt% of N,N-dicyclohexylmethylamine residue [59]. The residue level may depend on the extraction temperature. For example, 4 - 8 wt% at room temperature and 18 - 24 wt% at high temperature of DMCHA was observed in lipid extraction from microalgae [24]. In viscous heavy oil extraction using DMCHA, ap-

proximately 12 wt% DMCHA was found in the extracted oil, which can be reduced to 8 wt% with strong stirring conditions [21]. A similar extraction with another SHS (N, N, N', N'-tetraethyl-1,3-propanediamine) yielded residual content of 14 wt%, and 17 wt% with higher water content [82]. Until now, the predominant strategy used to reduce the solvent residue has been to expand the range of SHSs to find more efficient solvents [12, 13]. However, no systematic work has been done to optimize the switching conditions and to understand their influence on the amount of the residual solvent.

1.3 Thesis objectives

The overall goal of this thesis is to quantitatively understand the dissolution dynamics of binary SHS/polymer droplets and the influence of switching conditions on the residual solvent left in polymer particles. The individual objectives of this thesis work are the following:

1. Follow the dissolution of sessile binary SHS/polymer drops, and quantify the influence of the drop composition and trigger concentration on the drop lifetime.

2. Characterize the internal state of the drops during the dissolution process.

3. Visualize the resulting particle structure and comprehend the process that led to the structure.

4. Establish an experimental method to extract the residual solvent from the particles, and quantify it using Raman spectroscopy.

5. Produce and characterize latexes via SHS switching using a controlled experimental setup for the trigger addition.

6. Quantify the residual solvent inside of the recovered polystyrene, and investigate the influence of trigger concentration, trigger addition rate, emulsion composition, temperature and trigger type on the residual solvent.

1.4 Thesis outline

Chapter 1 introduces the background related to this thesis. The notion of SHSs and trigger are explained, and the working mechanism behind SHSs is given. Applications and benefits of SHSs are reviewed, and the studies related to the drop dissolution dynamics in the literature is presented for both single and multi component drops. This chapter also gives the motivations and objectives of this thesis.

Chapter 2 provides the experimental procedures for the single drop dissolution, powder formation, characterization, and residual solvent quantification used to obtain the results from Chapter 3 and 4.

Chapter 3 studies the dissolution of a binary DMCHA/polystyrene sessile drop immersed in a controlled acidic aqueous solution environment. This chapter aims at understanding the reaction-induced mass transfer of the SHS from the drop to the aqueous phase. We find a scaling relationship between the drop dissolution time and the initial size of the drop, and study the impact of the aqueous phase pH and initial drop composition on this scaling law. We also follow the internal state of the drop during the dissolution process, and show the existence of a phase separation and precipitation behavior, and its implication on the final morphology of the final polymer particle.

Chapter 4 focuses on studying the effects of extraction conditions on the amount of residual solvent inside of a polymer latex. DMCHA/polystyrene droplets are dispersed in an aqueous phase containing sodium dodecyl sulfate (SDS) as the surfactant to form an emulsion. An acidic solution is added to the emulsion at a fixed rate to precisely control the switching dynamics. This chapter compares the solvent residue levels at different trigger addition rates, trigger solution concentrations, organic phase fractions, emulsion temperatures and with different trigger types.

Chapter 5 summarizes the results and findings from this thesis. This chapter also gives potential interesting future works to extend the knowledge from this thesis.

Chapter 2

Methods and procedure[1]

2.1 Methods and procedure for Chapter 3

2.1.1 Materials, solutions and substrates

The SHS polymer solutions were prepared using a mixture of N-N Dimethylcyclohexylamine (Sigma-Aldrich, 99%, DMCHA) and polystyrene (Sigma-Aldrich, $M_w = 40\,000$ g/mol, beads, >99%). The weight ratio ranged from 10 to 30 wt% of polystyrene. Both chemicals were mixed under ambient condition in sealed vials using a magnetic stirrer for 2 hours until complete dissolution of the polystyrene beads in DMCHA. Acid solutions were freshly made before each dissolution using formic acid (Sigma-Aldrich, > 95%) and (Milli-Q) water. The solution concentration used in this work ranged from 1.1×10^{-1} M to 2.7×10^{-4} M (0.4 vol% to 0.001 vol%). The pH of the solutions was measured using a benchtop pH meter (Fisher Scientific, Accumet AE150) and ranged from 2.37 to 3.83. Small square ($1\ cm \times 1\ cm$) silicon substrates were cut from wafers and thoroughly rinsed with water, ethanol and then sonicated for 20 minutes with ethanol before finally being dried with a stream of air. The partial solubilities of DMCHA in water as well as water inside of DMCHA were measured by

[1]This chapter contains modified part of (1) published work by **Billet Romain**, Binglin Zeng, James Lockhart, Michael Gattrell, Hongying Zhao, Xuehua Zhang. 'Dissolution Dynamics of a Binary Switchable Hydrophilicty Solvent - Polymer Drop into an Acidic Aqueous Phase'. Soft Matter, 2022, and (2) Manuscript under preparation by **Billet Romain**, Binglin Zeng, Hongyan Wu, James Lockhart, Mike Gattrell, Hongying Zhao, and Xuehua Zhang. "Effects of Switching Conditions on Switchable Solvent Residue in Polystyrene Microparticles from Emulsion Extraction".

Table 2.1: Experimental parameters to study the influence of the initial drop composition, the pH in the aqueous phase is fixed at 2.53.

Initial polystyrene (wt%)	0									10					
Drop volume (μL)	0.15	0.20	0.35	0.50	0.55	0.65	0.80	2.30	4.25	0.25	0.40	0.55	0.70	0.90	1.20
Initial polystyrene (wt%)	10				20										30
Drop volume (μL)	2.00	2.40	2.95	3.65	0.30	0.45	0.70	0.85	0.95	1.45	2.20	2.55	3.00	3.25	0.35
Initial polystyrene (wt%)	30														
Drop volume (μL)	0.75	1.00	1.30	1.50	2.10	2.40	2.75	2.85							

progressively adding one compound in a vial of the other until saturation. A solubility of DMCHA in water of $15.3 \pm 1.7\ g/L$ and water in DMCHA of $155 \pm 7\ g/L$ (18.3 ± 0.8 vol%) were measured close to what was previously reported in the literature. [83]

2.1.2 Drop dissolution

To study the dynamics of this dissolution, a side view camera was used to record the drop dissolution. The drop dissolution setup is shown in Fig. 2.1. The substrates were placed at the bottom of a glass cuvette (Krüss Scientific, $36 \times 36 \times 30\ mm\ W \times D \times H$). The polymer solution was then filled in a glass syringe that was controlled by a connected Drop Shape Analyzer instrument (DSA-100, Krüss Scientific).

For each experiment, the glass cuvette was filled with 30 mL of the acidic solution. Drops of initial volume ranging from 0.15 to 3.65 μL were introduced by the motorized syringe on the surface of the substrate inside the aqueous acidic phase. In total, 70 dissolution conditions were studied, as summarized in Table 2.1 for the polystyrene content parameter and in Table 2.2 for the pH levels. During the drop dissolution, the side view images were captured directly by the DSA-100 with a 9x magnification. For the top view, an upright optical microscope (Nikon H600l) equipped with a 4x magnification lens and a camera was used to image the drops.

After the drop dissolution, the substrate was carefully removed from the acidic solution. The excess water on the sample was gently blown with air and the remaining water left to dry under ambient conditions for 48 hours.

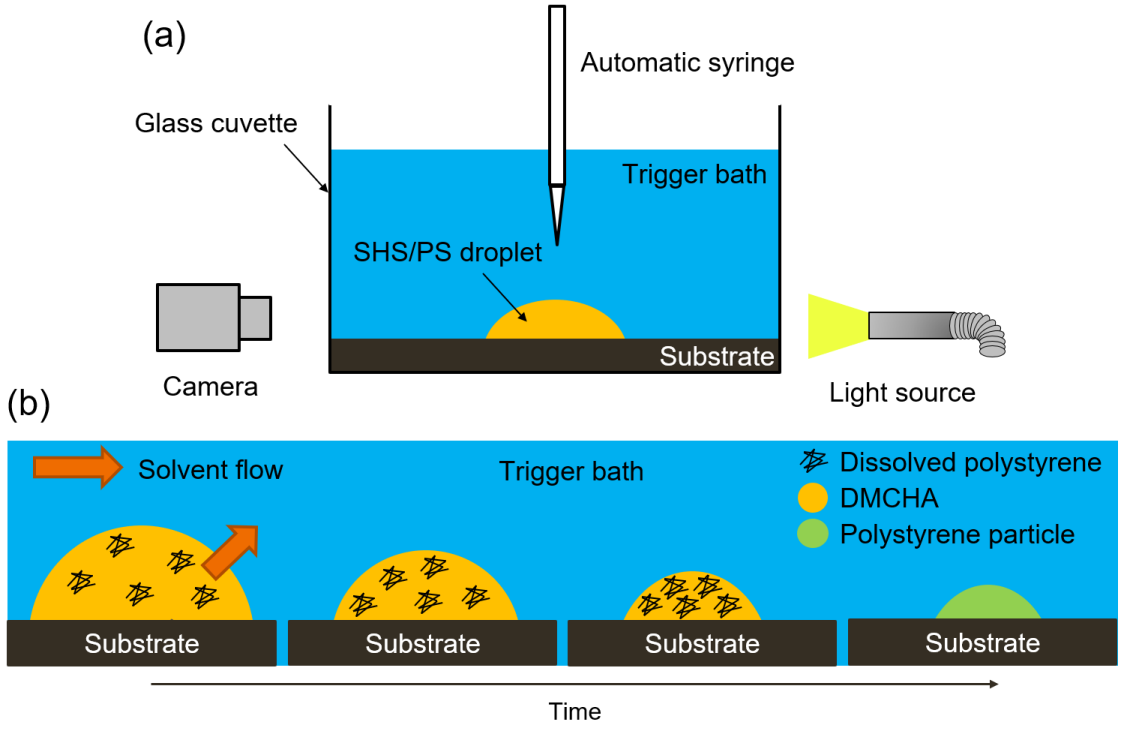

Figure 2.1: (a) Sketch of the single drop dissolution experimental setup. The binary DMCHA/polystyrene drop is placed on a silicon substrate inside a cuvette filled with formic acid solution using a motorized automatic syringe. The side view imaging is done with the help of a side camera and a light source passing through the drop. (b) Schematic depiction of the drop dissolution process. DMCHA is extracted out of the drop until only a polystyrene particle remains.

Table 2.2: Experimental parameters to study the influence of the trigger concentration, the initial polystyrene composition of the drop is fixed at 10 wt%

Aqueous phase pH	3.83					3.05									
Drop volume (μL)	0.20	0.60	1.35	1.70	2.60	0.15	0.40	0.45	0.75	1.10	1.40	1.75	2.00	2.85	3.20

Aqueous phase pH	2.53										2.37					
Drop volume (μL)	0.25	0.40	0.55	0.70	0.90	1.20	2.00	2.40	2.95	3.65	0.15	0.60	1.20	1.80	2.20	2.85

2.1.3 Image analysis and characterization

Video footage of the drops was analyzed using MATLAB. The MATLAB code used analyzed each frame of the side view videos and detected the drop using an intensity threshold. The detected drop was then used to measure the quantities of interest. This can be done either by assuming a spherical model and fitting a spherical-cap shape to the contour of the drop, which allows access to the contact angle of the drop, or by the 180° symmetric rotation of the drop section observed to obtain a volume. However, at the end of the dissolution process, the drop deviates from the spherical model due to the pinning and deformation of the drop. Therefore, we use the rotation to calculate an approximation of the drop volume. The final particles micro-structure and surface state were characterized by SEM (Zeiss Sigma FESEM). A theoretical final to initial volume ratio was calculated assuming (i) the complete removal of DMCHA from the particle, (ii) the absence of any porosity, and (iii) by approximating the DMCHA/polystyrene mixture density with a combination of the density of its pure constituents $\frac{1}{\rho_{mix}} = \frac{x_{DMCHA}}{\rho_{DMCHA}} + \frac{x_{PS}}{\rho_{PS}}$, with ρ_{mix} the DMCHA/polystyrene solution density, ρ_{DMCHA} and ρ_{PS} respectively the pure DMCHA and polystyrene density, and x_{DMCHA} and x_{PS} respectively the mass fraction of DMCHA and polystyrene. For a 90/10 wt% DMCHA/polystyrene solution, the approximated mixture density is $\rho_{mix} = 0.863\ g/cm^3$, very close to the density measured experimentally at 0.855 ± 0.004. The relative difference observed between the model and the experiment is 0.94% confirming the accuracy of the assumption.

2.2 Methods and procedure for Chapter 4

2.2.1 Chemicals and emulsion preparation

SHS/polymer solution was prepared using a 90:10 wt% mixture N-N Dimethylcyclohexylamine (Sigma-Aldrich, 99%, DMCHA) and polystyrene (Sigma-Aldrich, M_w = 40 000 g/mol, beads, 99%). Both chemicals were mixed at room temperature in

sealed vials for 2 hours resulting in complete dissolution of the polystyrene. The aqueous phase was made using a 3 wt% solution of sodium dodecyl sulfate (Sigma-Aldrich, 98.5%, SDS, surfactant) in water. In a typical emulsion formation, a controlled amount of organic phase, 6 to 18 g of 90:10 DMCHA:polystyrene solution was added to the aqueous phase, 54 to 42 g of 97:3 SDS solution. The organic phase fraction was used as a studied parameter and ranged from 10 to 30 wt% of the total emulsion weight. The organic phase was slowly added to the aqueous phase under magnetic stirring at 300 rpm to form a milky emulsion. Some polystyrene precipitated during the emulsion production and was removed prior to emulsion switching. The precipitated polystyrene was attributed to the high water solubility in DMCHA measured to be 18.3 $\pm$ 0.8 vol%. Water acts as a polystyrene non-solvent, lowering its solubility in the DMCHA phase and causing polystyrene precipitation.

2.2.2 Switching of the emulsion

Formic acid (Sigma-Aldrich, 95%) and sulfuric acid (Fisher scientific, 95%) solutions as well as dry ice were used as triggers to switch the emulsion. Acidic solutions were freshly prepared before each experiment in sealed vials under magnetic stirring for 10 minutes. Sulfuric acid solutions (1 M) were left to cool down to ambient temperature before usage. As shown in Fig. 2.2(a), a fixed volume of DMCHA/polystyrene emulsion (60 mL) was placed inside of a beaker under magnetic stirring at 300 rpm, while the same volume of trigger solution (60 mL) was loaded inside of a plastic syringe. The acidic solutions were then added at a controlled rate using a syringe pump until complete depletion of the syringe. For dry ice, small pieces of ice (1g) were progressively added every 2 min to the emulsion until 40 g of ice was introduced. The emulsion was kept partially sealed to prevent any pressure build-up. The temperature of the emulsion was controlled using a water bath, and the temperature of the emulsion was measured with a thermocouple to ensure the homogeneity of the temperature inside of the emulsion. For the formic acid trigger solution, the study

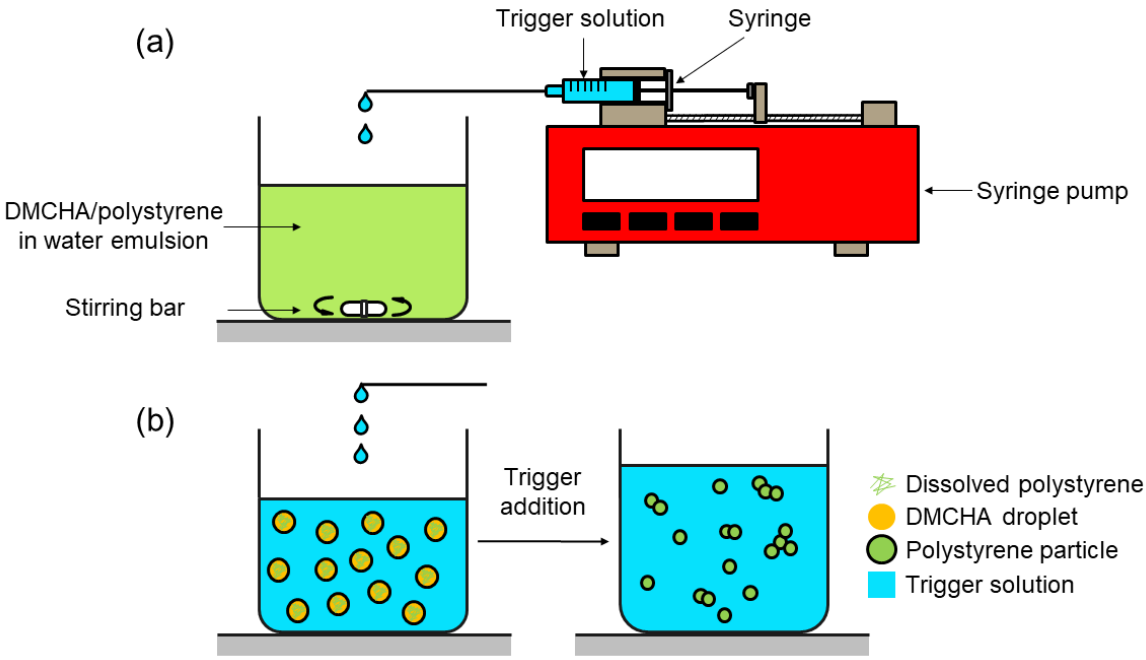

Figure 2.2: (a) Sketch of the experimental setup. An emulsion of DMCHA/polystyrene in water is placed inside of a beaker under constant magnetic stirring. An acidic trigger solution is then added at a fixed rate using a syringe pump. (b) Schematic depiction of the emulsion switching process. DMCHA inside of the SHS/polymer drops is switched to its hydrophilic form and solubilized in the aqueous surrounding leaving only polystyrene as particles.

Table 2.3: Experimental parameters studied for effects from the formic acid trigger. The parameters in the experiments are formic acid concentration in the solution, total trigger addition duration, emulsion composition and emulsion temperature.

No.	Total trigger addition duration (min)	Formic acid concentration (M)	Organic fraction emulsion (wt%)	Temperature (°C)
1	7.5/15/30/60/80/120/240/600	2.5	20	20
2	120	2.5/3.1/3.8/4.4/5	20	20
3	120	2.5	10/15/20/25/30	20
4	120	2.5	20	15/20/30/35/40/50/60/70/90

parameters include the solution concentration, total trigger addition duration, organic fraction in the emulsion and emulsion temperature. As listed in Table 2.3. The majority of the polystyrene was recovered as a powder after the emulsion switching process. However, when the temperature was high or the amount of organic phase in the emulsion was minimal, polystyrene aggregates developed alongside the powder. In these situations, the resultant solid polystyrene chunk could account for up to 50 wt% of the recovered polystyrene.

2.2.3 Powder filtration and imaging

Once the trigger solution addition finished and the solvent was switched, the polystyrene dispersion was filtered using vacuum filtration (Q2 filter paper, Fisherbrand, particle retention > 2 μm) to separate the polystyrene powder. The powder was washed using 100 mL of a 0.9 M sulfuric acid solution to get rid of the DMCHA left at the surface of the polystyrene powder. The powder was then left to dry for 24 hours at room temperature. For imaging purposes, a trace amount of nile red (Thermo Scientific, 99%) was used to dye the organic phase of the emulsion. The resulting powder could therefore be imaged under Confocal Laser Scanning Microscopy (DMi8 S, Leica Microsystems) with a 20x dry objective. The size distribution of the initial emulsion and final dispersion was collected using a Focused Beam Reflectance Measurement probe (FBRM G400, Mettler Toledo).

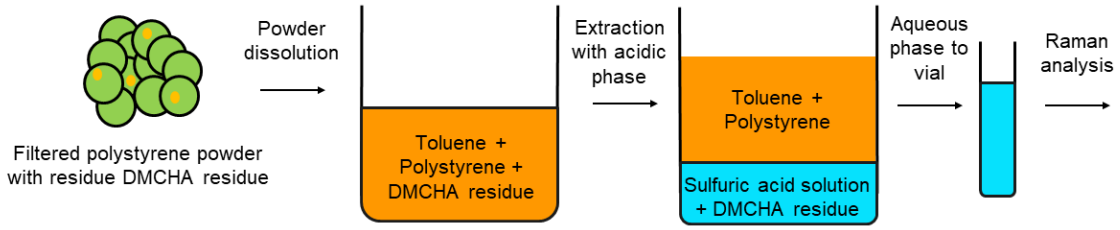

Figure 2.3: Residual DMCHA extraction process for the powders obtained from the DMCHA/polystyrene emulsion switching. The powder is dissolved in toluene. An acidic aqueous phase is then added and mixed to extract the residual DMCHA. The aqueous phase is then transferred to a vial and analyzed using Raman spectroscopy.

2.2.4 Extraction and quantification of the solvent residue

To quantify the solvent residue inside of the powder, DMCHA was extracted from the polystyrene into an acidic aqueous phase as presented on Fig. 2.3. Firstly, the polystyrene powder was weighted on a micro balance and then dissolved into 40 mL of toluene inside of a beaker under magnetic stirring. Secondly, 5 mL of 0.9 M sulfuric acid solution was added as the extracting phase for DMCHA from the toluene phase. The two phases mixture was then left mixing for 8 hours. Once the mixing stopped and phase separation was completed, 3 mL of the aqueous phase was transferred to a vial. The aqueous phase was then analyzed in the vial using a handheld Raman specvtrometer device (Cora 100, Anton Paar, 785 nm). Intensity was kept on high settings with a 20s exposure time. The results were then exported and baseline corrected using splines to fit to the baseline.

Chapter 3

Dissolution Dynamics of a Binary Switchable Hydrophilicity Solvent - Polymer Drop into an Acidic Aqueous Phase[1]

3.1 Results

3.1.1 Morphology of a dissolving binary SHS/polymer drop

The dissolution process was recorded and then the videos were converted into image frames vs time. Fig. 3.1(a) presents a typical dissolving process of a drop. The initial composition in the drop was 90:10 wt% DMCHA:polystyrene dissolved in a formic acid solution of pH = 2.53. In the first snapshot, we show the baseline which corresponds to the contact line between the drop and substrate. Using a spherical-cap shape model, we fit a circle to the rim of the drop, allowing to define several quantities to describe the drop state. D is defined as the contact diameter and H as the height of the drop. We also define θ as the contact angle, the tangential angle of the circle at the baseline intersection. The time t = 0 is taken at the start of the recording, which corresponds roughly to the time of the drop deposition with a time difference of around 5s, negligible compared to the total time of dissolution $\sim$

[1]This chapter contains modified part of published work by **Billet Romain**, Binglin Zeng, James Lockhart, Michael Gattrell, Hongying Zhao, Xuehua Zhang. 'Dissolution Dynamics of a Binary Switchable Hydrophilicty Solvent - Polymer Drop into an Acidic Aqueous Phase'. Soft Matter, 2022.

3,000s. At the beginning of the dissolution, the drop exhibits a spherical-cap shape that allows to clearly define the contact angle (t = 0 - 3,000s). For a 90/10 wt% DMCHA:PS drop in a solution of pH = 2.53, an initial contact angle $\theta_0 = 53 \pm 3$ is found. However, approaching the end of the dissolution (t = 3,000 - 3,500s), deformation starts to appear and the drop deviates from the spherical-cap shape model. Therefore, throughout this step, the measurement of a contact angle becomes less accurate. The morphology deformation may also correspond to the shift from the liquid drop to the solid particle and so the contact angle at this time would no longer have a meaning related to the liquid properties. Following this, the dissolution ends and no further changes can be observed. During the dissolution process, the drop contact diameter shrinks from 2.7 mm to 1 mm. However, the contact angle increases by 30° between the initial and final state.

Fig. 3.1(b-c) shows the measured contact diameter D and drop height H against the dissolution time t. The contact diameter remains constant at D = 2.7 mm from t = 0 to t = 1,000s as the drop boundary is pinned on the surface. Then, the contact diameter decreases during the remaining of the process (1,000s < t < 3,500s). The height of the drop decreases from 0.8 mm to 0.5 mm during almost the entire process. At first, we observe a sharp drop of H during the constant contact diameter step from t = 0 to t = 1,000s, and then a slow decrease from t = 1,000 s to t = 3,000s. Afterward, morphology change of the drop sometimes induces a slight height increase.

Fig. 3.1(d) shows the change in calculated volume V of the drop. As we only have snapshots of a side view, we assume a 180° rotational symmetry of the drop around its center. We can therefore calculate the drop volume by measuring only the surface area of the observed drop section. This hypothesis is confirmed by the top view imaging, and only deviates slightly from the symmetric model during the deformation step. Throughout the entire dissolution process, the calculated volume of the drop decreases from 2.4 μL to 0.3 μL. The final volume is approximately 12.5% of the initial volume, which is close to the calculated ratio of 12.2% based on

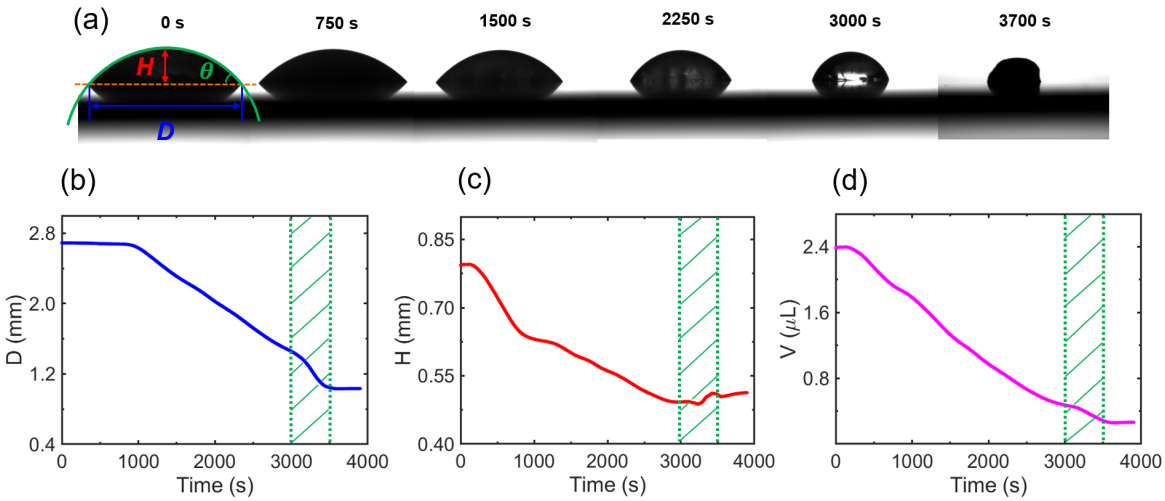

Figure 3.1: (a) Snapshots of a 2.4 μL, 90:10 wt% DMCHA:polystyrene drop inside of an aqueous acid solution of pH 2.53 at different times during the dissolution process. The dashed orange line corresponds to the contact line between the drop and the substrate. The curved green line shows the fitting of the drop to a spherical model. H is defined as the height of the drop, D shows the contact diameter and θ is the contact angle of the drop. (b-d) Plots of different parameters of the drop (Contact diameter (b), height (c) and volume (d)) measured and calculated via image analysis against the dissolution time. The green dashed zone corresponds to the observed morphology deformation phase when the liquid drop transitions to a solid particle.

the initial drop volume and polymer mass fraction.

3.1.2 Dependence of dissolution on initial drop volume

A series of dissolution experiment was performed to study the influence of different parameters on the drop shrinking dynamics, including the polystyrene content and acidic solution pH. The first analyzed parameter is the initial drop volume. The drop volumes range from 0.25 μL to 3.65 μL. Fig. 3.2(a-d) shows snapshots of the dissolution of 90:10 wt% DMCHA:polystyrene drops in a formic acid solution of pH = 2.53 with different initial volumes. As expected, the lifetime of smaller drops is shorter than that of bigger drops. The timescale of the dissolution can be as short as 950s ($\sim$ 16 min) for the smallest drops (0.25 μL) and as long as 4700s ($\sim$ 78 min) for the largest drops (3.65 μL).

To quantify the dissolution process dynamics, we introduce a scaling law. The

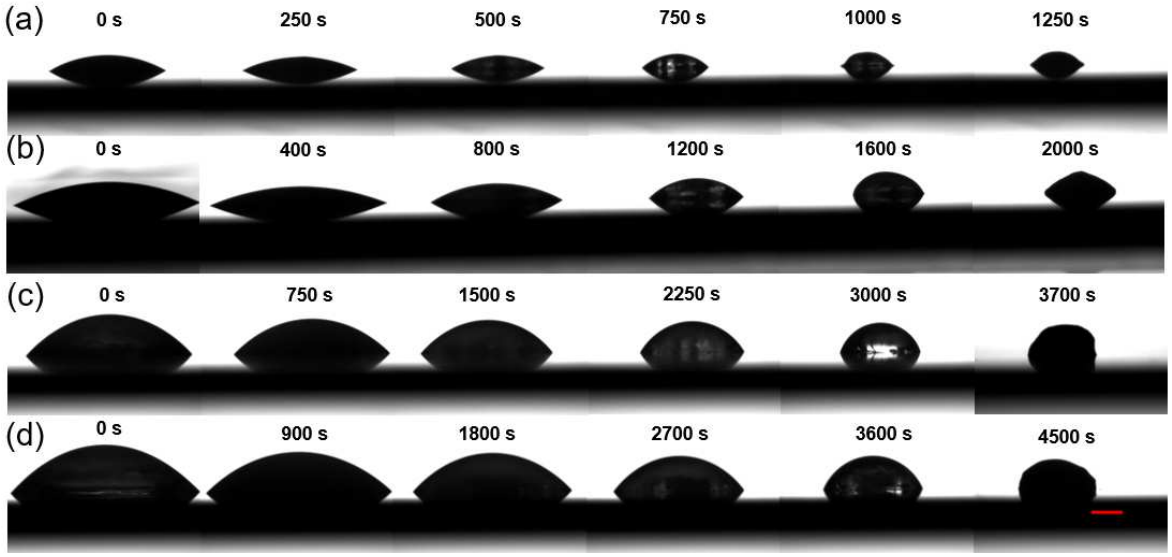

Figure 3.2: (a-d) Snapshots during the dissolution process of different initial drop volume (from (a) to (d) 0.25, 0.90, 2.40 and 2.95 μL). The drops all have a 90:10 DMCHA:polystyrene initial composition and are dissolving inside of an aqueous acidic environment of pH = 2.53. Smaller drops are dissolving faster than larger drops. The length of the scale bar is 0.5 mm.

initial volume of the drop V_0 is defined as the measured volume at the time t = 0. We also define the lifetime τ of the drop, which corresponds to the time when the measured volume V becomes constant as a function of time, and correlates to the time when the dissolution is finished and no changes can be observed anymore (less than 0.01% of volume change per second for a minimum of 30s). We relate τ and V_0 with the following scaling law:

$$\tau = \alpha * V_0^{\gamma} \tag{3.1}$$

The coefficient α is a prefactor whereas γ is a scaling coefficient.

Fig. 3.3(a) shows the volume curves as a function of the dissolution time. We then extract from the volume curves the drop initial volume V_0 and lifetime τ which are then used to deduce the scaling law presented in Fig. 3.3(b). A scaling coefficient γ of ~ 0.60 and prefactor α of ~ 2200 are found from the curve fitting to our scaling model.

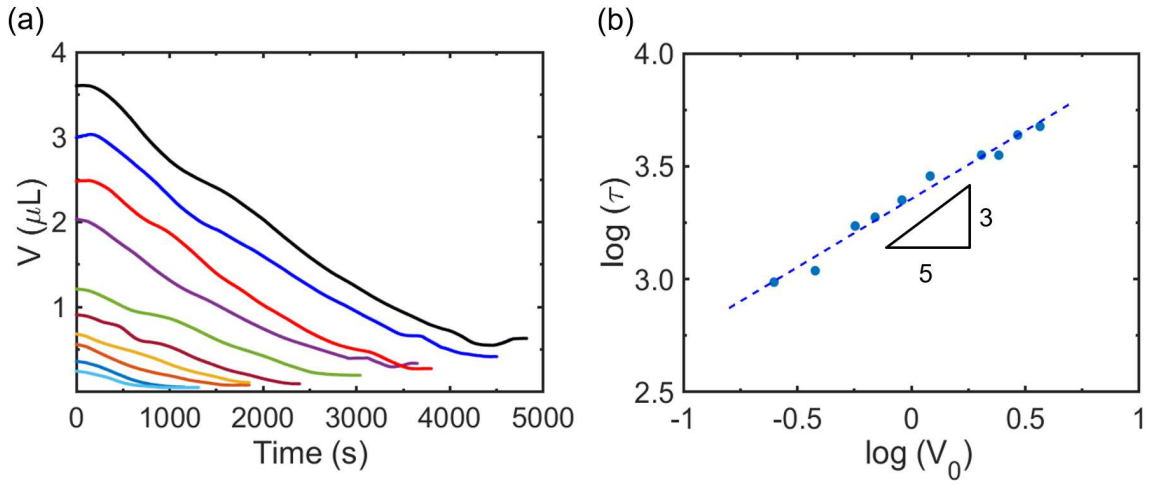

Figure 3.3: (a) Calculated volume as a function of the time for drops with different initial volume V_0. The drops all have a 90:10 DMCHA:polystyrene initial composition and are dissolving inside of an aqueous acidic environment of pH = 2.53. (b) Scaling law as a log-log plot of the drop lifetime τ as a function of the initial volume V_0. Points are extracted from (a) and a line of equation $\gamma x + b$ is fitted to the experimental data. The slope is the scaling coefficient γ and the intercept b is related to the prefactor with $\alpha = 10^b$

3.1.3 Influence of the initial drop composition and trigger concentration

We study the impact of the initial drop composition and the trigger concentration on the dissolution process by fixing one parameter and changing the other. Video footages of the dissolution of 6 to 12 drops of different initial volume are analyzed.

Firstly, we fix the trigger concentration to study the impact of the initial drop composition. The pH of the aqueous solution is fixed at 2.53, while initial drops contain 10, 20 and 30 wt% of polystyrene. The plot of τ against V_0 is presented Fig. 3.4(a). We can see that the fitted lines for different polystyrene concentrations in the drop are almost parallel, suggesting similar scaling coefficient γ, as it is summarized in Fig. 3.4(b). The scaling coefficient seems to be constant against the change in polystyrene initial concentration, and a mean scaling coefficient $\gamma = 0.52 \pm 0.07$ is found. However, the line fittings differ in the prefactor as shown in Fig. 3.4(b). A trend is that the prefactor decreases with an increase in polystyrene initial concen-

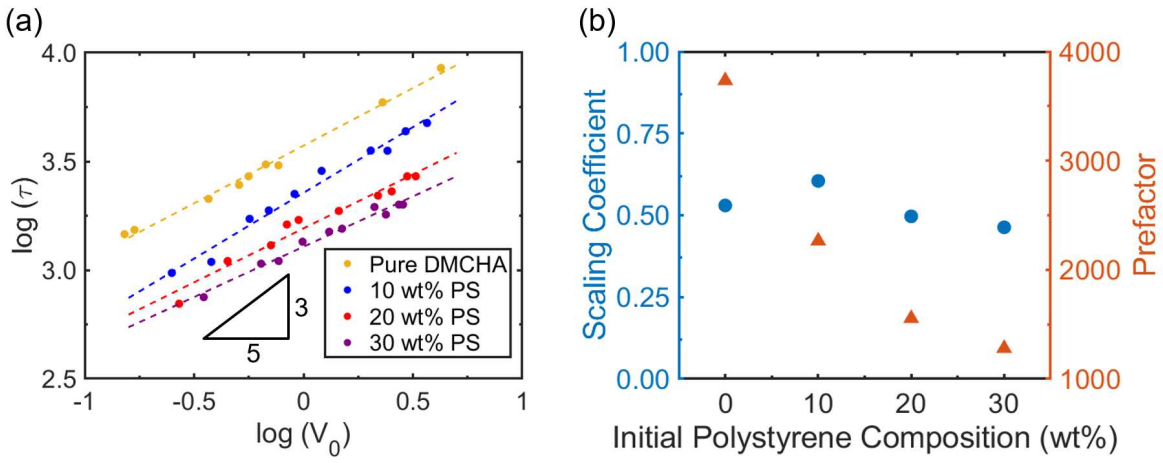

Figure 3.4: (a) Scaling laws as a log-log plot of the drop lifetime τ as a function of the initial volume V_0 for different initial drop composition. The polymer solutions used are from top to bottom, pure DMCHA, 10, 20 and 30 wt% of PS. Every point represent one drop dissolution. (b) Scaling coefficients (left) and prefactors (right) extracted from the scaling laws as a function of the initial polystyrene composition in wt%.

tration. This physically means that the higher the initial polystyrene concentration is, the faster the same-sized drop dissolution will finish.

We also study the impact of the trigger concentration by fixing the initial drop composition. During the experiments, the polymer solution concentration used to make the drop is maintained at 10 wt% of polystyrene. We change the trigger concentration inside of the aqueous phase from 0.001 vol% to 0.4 vol% of formic acid (pH = 3.83 to pH = 2.37). The pH of the solutions were chosen to match the pH of carbonated water under CO_2 pressures ranging from 1 to 10 bar [84, 85]. The resulting τ against V_0 is presented Fig. 3.5(a). Again, we can see that the fitted lines are nearly parallel. We observe an almost constant scaling coefficient in Fig. 3.5(b). The mean scaling coefficient γ is $\gamma = 0.54 \pm 0.07$. Similarly to the drop initial composition parameter, the fittings differ by their prefactor, as summarized in 3.5(b). A higher trigger or formic acid concentration results in a lower pH and lower prefactor. Therefore, at lower pH, the dissolution process proceeds faster than at higher pH.

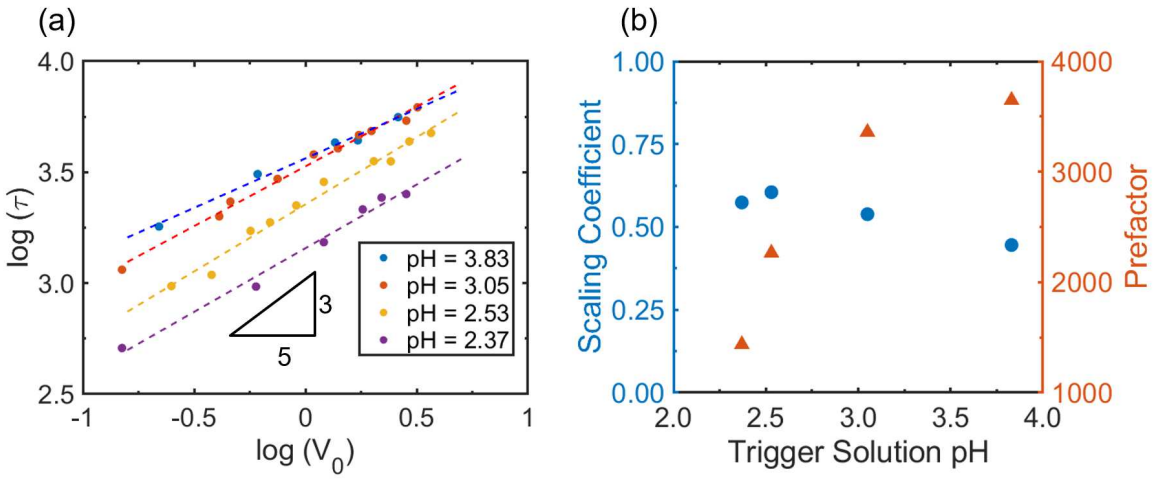

Figure 3.5: (a) Scaling laws as a log-log plot of the drop lifetime τ as a function of the initial volume V_0 for aqueous solution pH. From top to bottom, the pH of the aqueous extracting phase is 3.83, 3.05, 2.53 and 2.37. Every point represents one drop dissolution. (b) Scaling coefficients (left) and prefactors (right) extracted from the scaling laws as a function of the aqueous solution pH.

3.1.4 Internal view of the dissolution process

To complete the dissolution process observation, we setup a top view camera. This top view experiment allows us to discern the internal structure and flow in the drop during the extraction of DMCHA. Fig 3.6(a) presents snapshots at different stages during the dissolution of a 90:10 DMCHA:polystyrene drop inside of an acidic solution of pH 2.53.

When the drop is introduced in the trigger bath, multiple phases can be observed. Once the dissolution starts, three phases are observed within the drop: a solid polystyrene phase at the center of the drop, small microdroplets moving radially inside of the liquid phaseof polymer and unswitched DMCHA. Such phase separation behavior appears during the early stage of the dissolution process and can be considered as almost instantaneous compared to the remainder of the drop shrinking.

As time passes, the main drop shrinks in accordance to what was observed with the side-view experiment. Some of the microdroplets seen inside of the main drop

join with the polystyrene aggregate in the center, leading to a change in the shape of the polystyrene core. Finally, the liquid outline of the main drop touches the edge of the polystyrene aggregate (t = 4min). At this time, deformation of the drop starts to occur, and the main drop boundary starts to coincide with the polystyrene core. During the remaining solvent dissolution, the drop finishes its deformation step resulting in the formation of the final polystyrene particle.

As we suspected the aqueous environment to saturate the drop with water and alter the solubility of polystyrene, we also examined a solution of DMCHA/polystyrene made from DMCHA pre-saturated with water. Water pre-saturated DMCHA did exhibit a much lower polystyrene solubility qnd wqs brought to saturation with polystyrene. During the mixing of water-saturated DMCHA with polystyrene, water microdroplets also separate from DMCHA and the system becomes an emulsion of water inside of the DMCHA/polystyrene solution. The emulsion is stable and takes as long as two days to separate. The saturated DMCHA drop dissolution is presented Fig 3.6(b). The drop pre-saturated with water and polystyrene, as opposed to the one without pre-saturation with water does not exhibit any internally precipitated polystyrene at the beginning of the dissolution. Water microdroplets coming from the emulsion range from 5 to 50 μm in diameter. During the shrinking, the microdroplets can be seen moving radially. The microdroplets also grow larger as they are coalescing with each other. Near the end of the dissolution process, the main drop starts to deform and at this step, a large number of small-scale microdroplets measuring less than 1 μm can be seen appearing Fig. 3.6(b) (t = 3.5 min). Some of the water droplets appear stay trapped in the particle as the dissolution process finishes.

3.1.5 Porous microstructure of the final particles

We also investigate the final surface state and microstructure of the particles resulting from the dissolution process using SEM. Multiple particles were prepared using drop composition and trigger concentration as parameters. Fig. 3.7(a-f) present SEM

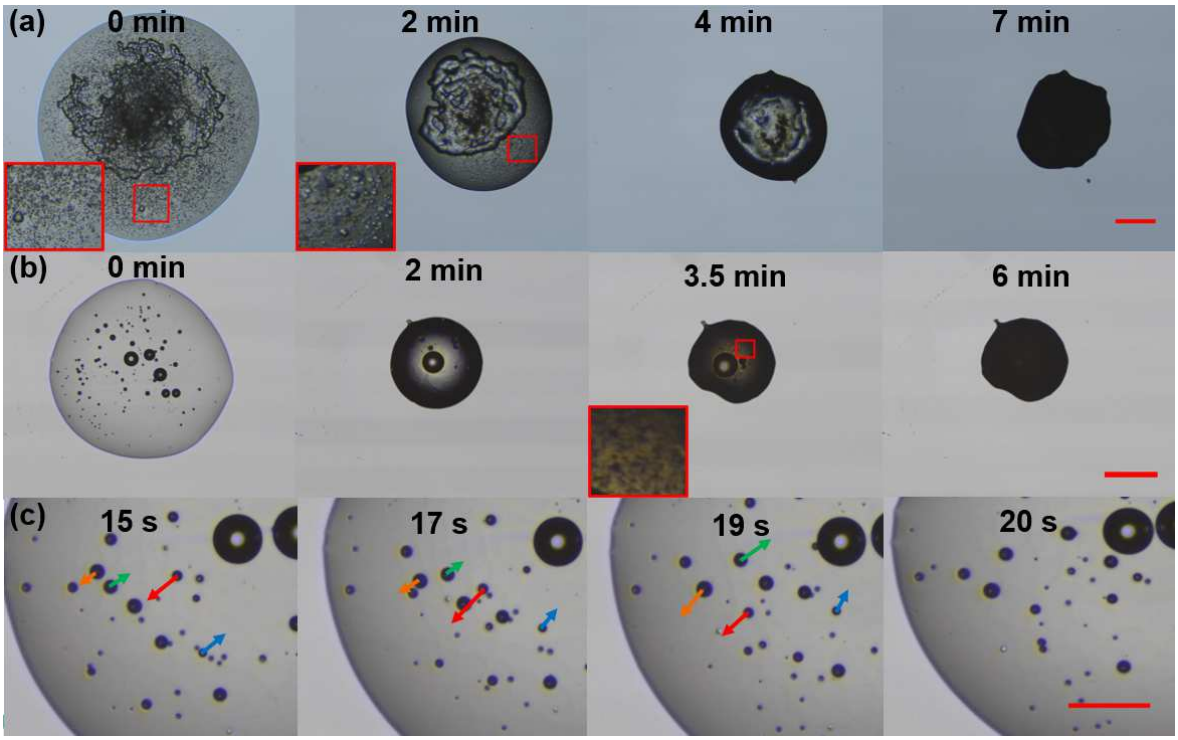

Figure 3.6: (a) Snapshots of a 90:10 wt% DMCHA:polystyrene drop observed from the top in an aqueous phase at pH 2.53 at different time during the dissolution. The drop internal state can be observed. At the center of the drop, a polystyrene precipitate is present and microdroplets can be seen moving along the radius of the principal drop. The scale bar corresponds to 200 μm (b) Snapshots of a DMCHA:polystyrene:Water drop at saturation observed from the top in an aqueous phase at pH 2.53 at different time during the dissolution. No polystyrene precipitates can be observed, however microdroplets of water can be seen moving along the radius of the main drop and coalescing during the dissolution. The scale bar corresponds to 200 μm (c) Zoom into the main water and polystyrene saturated drop. The water microdroplets move radially inside of the drop, going either to the rim or the center of the drop. The scale bar corresponds to 60 μm

images of 3 particles. We also examine the bottom surface of the particle, which corresponds to the portion of the particle in contact with the silicon substrate Fig. 3.7(g).

Firstly, the overall shape of the structure exhibit an almost spherical shape, even while changing the conditions of the dissolution. A slight pinning effect of the substrate is observed in the final shape of some of the particles. However, a difference in the surface state can be observed when the pH of the solution used is increased. For a high pH aqueous solution, the final particles exhibit a rougher surface at a macroscopic scale, while at low pH, the surface state seems to be smoother.

Another characteristic of the particles can be observed when looking at the microstructure of the particle. Some pores are observed at the micro-scale, with pores diameters ranging from 30 nm to 200 nm. We observe larger pores in structures starting with a lower polystyrene initial composition, resulting in smoother surfaces. On the opposite side, smaller pores are seen for higher polystyrene initial composition drops.

The bottom surface of the particle presented in Fig. 3.7(g) exhibits a smooth texture without pores or defects for the area around the center of the particle. However, at the rim of the particle, different defects such as cracks or wrinkles are observed. The size of the defects ranges from 10 μm to 100 μm. Once more, in the rim area of the particle, no pores can be observed when looking at micrometer scale.

3.2 Discussion

3.2.1 A switching-dissolution process

An interesting aspect in our DMCHA/polystyrene drop dissolution is the switching process at the drop surface by the acidic solution. DMCHA is sparsely soluble in water in neutral form, but highly soluble in protonated form. The main contribution to the dissolution is driven by the switching of DMCHA to $DMCHAH^+$.

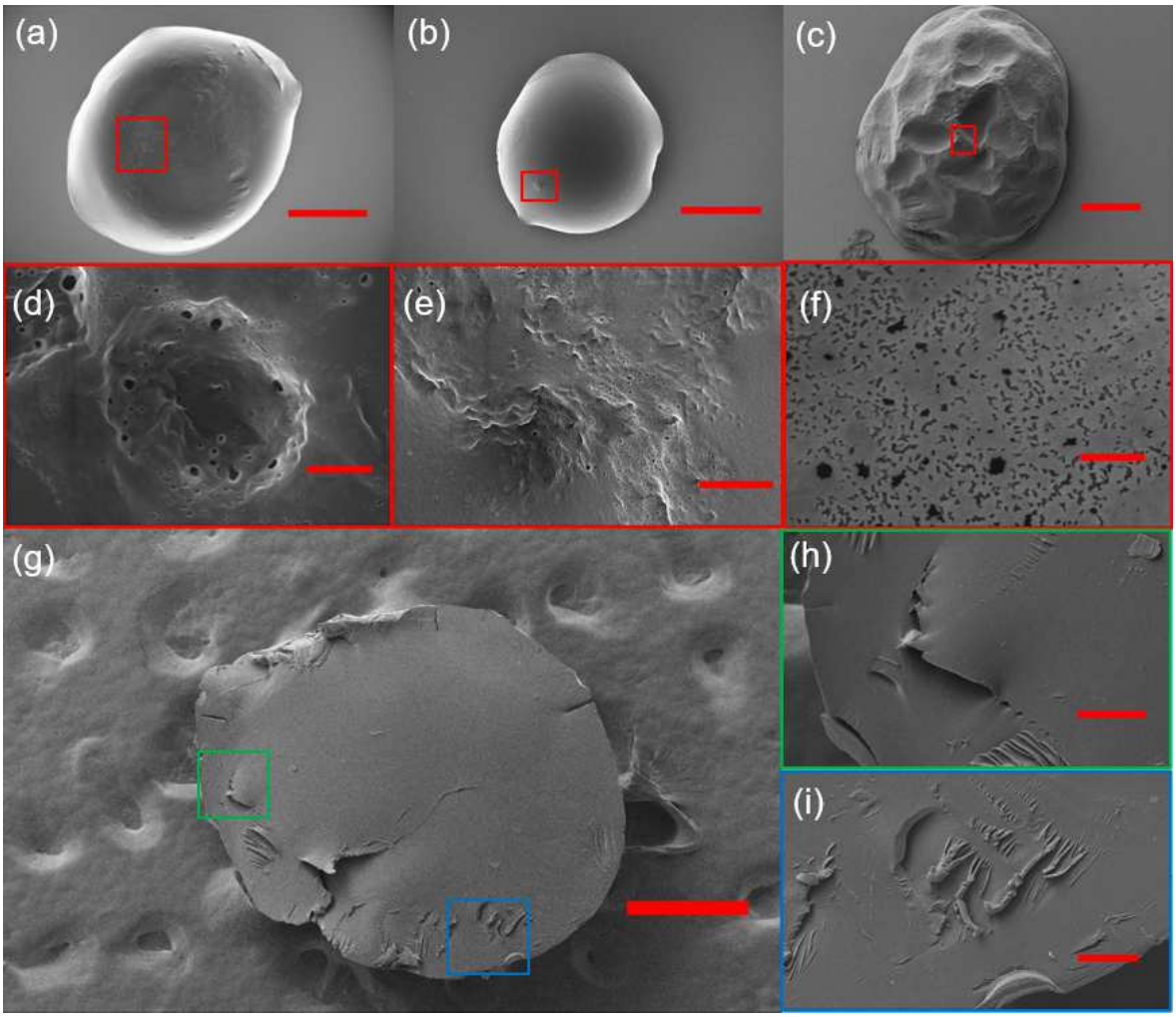

Figure 3.7: (a-c) SEM images of the final particle obtained after the drop dissolution process. From left to right, different conditions of drop dissolution have been applied, respectively, (a) 90:10 wt% DMCHA:polystyrene at pH 2.53, (b) 80:20 wt%, DMCHA:polystyrene at pH 2.53 and (c) 90:10 wt% DMCHA:polystyrene at pH 2.37 . Scale bars: 400 μm, 400 μm and 200 μm (d-f) Enlargment of the microstructure of the particles. A porous surface can be observed at the micrometer scale. Scale bars: 800 nm, 600 nm and 800 nm (g) Bottom surface of the particle previously in contact with the silicon substrate. The particle was produced with a 90:10 wt% DMCHA:polystyrene drop at pH 2.53. The particle is turned upside down. Enlargments of cracks (h) and wrinkles (i) observed at the rim of the particle are presented respectively in green and blue. Scale bars: 400 μm, 60 μm and 60 μm

$$c_s = [DMCHA^0]_{aq} + [DMCHAH^+]_{aq}$$

With $[DMCHA^0]_{aq}$ the natural solubility of neutral DMCHA in its environment, and $[DMCHAH^+]_{aq}$ the concentration of the protonated form of DMCHA. Here, the solubility of DMCHA can be split into two parts, and we can consider the solubility of $[DMCHA^0]_{aq}$ independent of the acid concentration. [14]

The dissolution of DMCHA is strongly dependent on the solution pH. The dissociation constant of DMCHA is expressed as

$$K_a = \frac{[H^+]_{aq}[DMCHAH^0]_{aq}}{[DMCHA^+]_{aq}} = \frac{10^{-pH}[DMCHAH^0]_{aq}}{[DMCHA^+]_{aq}} \tag{3.2}$$

An increase of the acid concentration results in an increase in $[DMCHAH^+]_{aq}$ amd therefore an increase in c_s. The mass transfer of solvent away from the surface of the drop will be related to the concentration difference between the surface of the drop and far away from the drop $\Delta c = c_{surface} - c_\infty$. For a fast reaction, the equilibrium is reached and the surface concentration corresponds to the DMCHA solubility c_s. The concentration far away from the drop can be neglected considering the size of the drop compared to the volume of the trigger bath. Therefore, the concentration difference between the surface and far away from the drop can be reduced to the DMCHA solubility. As an increase in solubility of DMCHA at lower pH drives faster dissolution, the lifetime τ of the drop is shorter when other conditions are fixed.

To compare the times scales of reaction and diffusion, we introduce the Damköhler number Da, defined as the ratio of the reaction rate to the diffusive mass transport rate. We assume first order kinetics in DMCHA and in H^+. The diffusive mass transfer rate can be derived from Fick's law. Therefore, the Damköhler number can be expressed with the equation below.

$$Da = \frac{k_s[DMCHA][H^+]_{aq}}{\kappa \Delta c D} \tag{3.3}$$

With k_s the reaction rate constant of the switching reaction, [DMCHA] the concentration of DMCHA in the drop and $[H^+]_{aq}$ the concentration of protons in the aqueous phase, κ the diffusion coefficient of DMCHA in the surrounding liquid.

According to other work [86], the recovery reaction of DMCHA follows a kinetic of the first order, with k_r the reaction rate constant of DMCHA recovery defined as $\frac{d[DMCHA]}{dt} = k_r[DMCHA] = -k_s[DMCHAH^+][H^+]$. The slowest recovery rate studied was $k_r = 4.2\times10^{-4}s^{-1}$. We calculate the switching reaction rate constant $k_s = \frac{k_r}{K_a}$, with K_a the dissociation constant of DMCHA. We find with these approximations a Damköhler number $Da = 1.7 \times 10^{12}$ in the case of an aqueous phase at pH 7, suggesting that diffusion is the rate-limiting step. Therefore in this work, we neglect the influence of the reaction on the shrinking dynamics of the drop.

3.2.2 Scaling law for drop dissolution

The simplest model that describes the dissolution process of a pure sessile drop driven by diffusion is [62]

$$\tau = A(\theta)\frac{\rho}{\kappa\Delta c}V_0^{\frac{2}{3}} \tag{3.4}$$

With $A(\theta)$ a geometrical constant depending on the contact angle θ (assumed constant), ρ the density of the drop material, Δc the difference between the concentration of the drop material at the drop interface and far away from the drop, and V_0 the initial volume of the drop. Following a diffusion mechanism, a scaling coefficient γ of $\frac{2}{3}$ is expected [60, 62, 63].

Convection in the surrounding liquid may enhance the drop dissolution. [68] A convective flow can be induced by the change in the liquid density along the surface of the dissolving drop. As a consequence of this density change, the density-altered layer is subjected to buoyancy or sinking, creating convection cells outside the drop, and enhancing the mass transport. For convection driven drop dissolution,

$$\tau = A'(\theta)(\frac{\nu\rho^4}{g\beta_c\Delta c^5\kappa^3})^{\frac{1}{4}}V_0^{\frac{5}{12}} \tag{3.5}$$

With $A'(\theta)$ a new geometrical constant depending on the contact angle, ν the kinematic viscosity of the surrounding liquid and g the acceleration of gravity. β_c is the solutal expansion coefficient defined by $\beta_c = \frac{1}{\rho_b}\frac{\partial\rho}{\partial c}$, with ρ_b the pure surrounding liquid density and $\frac{\partial\rho}{\partial c}$ the change in density of the surrounding liquid while a concentration c of the drop liquid is dissolved in it.

We calculate the dimensionless Rayleigh number associated with the dissolution process, quantifying the ratio of the diffusion time scale over the convection time scale. The Rayleigh number can be defined with the following relation [68]:

$$Ra = \frac{g\beta_c\Delta c(D/2)^3}{\kappa\nu} \tag{3.6}$$

Where g is the acceleration of gravity and all the other terms are defined as for the previous equations. The term $\beta_c\Delta c$ is simplified by the expression $\frac{\Delta\rho}{\rho_{water}}$, with $\Delta\rho = \rho_{water}^{saturated} - \rho_{water}$, the difference in density between water saturated with DMCHA and the pure water density. This term quantifies the alteration of the density of the aqueous liquid layer at the surface of the drop. Approximating the density of the mixture by the formula $\rho_{mix} = x_{DMCHA}\rho_{DMCHA} + x_{water}\rho_{water}$, we find a density difference of 2.2 $kg.m^{-3}$ at pH 7. The calculated Rayleigh number ranges from $Ra(D = 2mm) = 3.0 \times 10^4$ for large drops to $Ra(D = 0.2mm) = 30$ for particles at the end of the dissolution process. Both calculated Rayleigh numbers are above the threshold Rayleigh number of 12 found for dissolution of pure drops by Dietrich et al.[68].

The overall scaling coefficient γ found from the drop dissolution study is 0.53 ± 0.07. This coefficient is in-between the coefficient of the pure diffusion model γ of 0.67 and the convection-driven model γ of 0.42. The reason why the dissolution scaling coefficient is different than the convection dominated process may be that the

transport of DMCHA across the interface is inhibited by polystyrene in the drop. Effects from the insoluble component were also observed for the dissolution of other colloidal or polymer drops in the literature. [76, 78, 87, 88]

3.2.3 Effects of initial polystyrene concentration

The main difference observed when changing initial polystyrene concentration composition is the prefactor α. A higher initial polystyrene concentration in the drop means that for a given initial drop volume, less DMCHA was dissolved to complete the drop dissolution process, and, assuming the dissolution rate constant, a shorter lifetime or a smaller prefactor is expected.

On the other hand, the mass transfer of DMCHA is also dependent on how much DMCHA reacts at the aqueous interface. A high initial polystyrene concentration in the drop reduces the DMCHA concentration at the drop surface. The dissolution is slowed down and an extended lifetime of the drop can be expected. Shorter lifetime at higher polystyrene concentration suggests that the main effect from polystyrene is not the reduced DMCHA dissolution rate, but less DMCHA in the drop to dissolve before the polystyrene particle formed at the end.

3.2.4 In-drop phase separation and porous structure of particles

As the drop is immersed in the trigger solution, there is an influx of water through inter-diffusion into the drop. Water acts as a non-solvent for polystyrene in the drop, hence reducing greatly the solubility of polystyrene in the drop and resulting in fast precipitation of polystyrene from the initial contact with the trigger solution.

During the dissolution, DMCHA flows out from the drop, and the concentration of polystyrene in the drop increases. This change in polystyrene concentration decreases the water solubility inside the drop which then leads to water microdroplets formed from the oversaturation. These water microdroplets can exist for long time, possibly

attributed to the protonated form of DMCHA acting as a surface active species. The water microdroplets contained in the main drop are trapped during the transition of the dissolving drop to a polystyrene particle. Some of the microdroplets present at the surface during this transition create a porous structure at the surface of the particles.

It is interesting to note that there is polystyrene precipitation involved in the particle formation dynamics studied here. The time-limiting step for the particle formation is not the switching process, as the switching by protonation is extremely fast. As water penetrates into the drop, polystyrene precipitation is induced, which is also a relative fast step due to the small size of the drop. Apart from precipitation induced by water penetration, the slowest step in the entire particle formation is shrinkage of the drop from dissolution of the switched form, which is determined by drop size, and mass transfer into the surrounding.

The movement of the water microdroplets is reminiscent of the coffee-ring effect [89], recently shown to also exist in dissolving drops [90]. The large increase in viscosity of the main drop due to the increase in polystyrene concentration slows down the flow inside of the drop and fixes the water microdroplets.

3.3 Conclusions

In this work, we studied the dynamics and in-drop phase separation during the dissolution process of drops of SHS, water and polymer in a trigger solution. Switching DMCHA to the hydrophilic form at the drop surface led to the dissolution of the drops of DMCHA and polystyrene. An increase in both trigger concentration and initial polystyrene composition decreased the lifetime of the drop. The lifetime of the dissolving drops followed a scaling relationship between the drop lifetime and the initial drop volume. An overall scaling coefficient of 0.53 ± 0.07 was found based on 70 different initial conditions, suggesting that the dissolution rate was in-between the diffusion-dominated and convection driven dissolution. Along with drop dissolution,

water intake into the drop led to in-drop precipitation of polystyrene as water acts as a non-solvent for polystyrene. Water microdroplets formed through in-drop nucleation from reduced solubility of water in concentrated drops, and contributed to the porous microstructure of the final polystyrene particle.

A challenge related to the application of SHS such as the formation of latex [59] or extraction of bitumen [21] is how to remove SHS efficiently during switching processes. An improved understanding of the mechanism underlying the drop dissolution, internal drop dynamics and final structure formation may be useful for rational design of the switching procedures for reduced solvent residue and desirable properties of the final particles.

Chapter 4

Effects of Switching Conditions on Switchable Solvent Residue in Polystyrene Microparticles from Emulsion Extraction[1]

4.1 Residue extraction and quantification

An initial goal was to establish a sensitive method for quantification of DMCHA residue in solid PS particles. To do this, the PS prepared from emulsion extraction is first dissolved into toluene, then DMCHA is extracted from the PS and toluene solution to an acidic aqueous phase. Following that, the amount of extracted DMCHA was quantified using Raman spectroscopy and a reference calibration curve.

To establish a calibration curve, a controlled amount of pure DMCHA is injected in a fixed amount of toluene. The SHS is then extracted using a 0.9 M sulfuric acid solution. The aqueous phase is then analyzed by Raman spectroscopy. The extraction is repeated several times with controlled amounts of DMCHA injected in the toluene phase. Fig. 4.1(a) shows the Raman spectra of the aqueous phase after extraction with 0.3 to 2.3 g/L of DMCHA in the toluene phase. The most prominent peaks in Raman spectra situated at 440, 590, 890, 982 and 1050 cm^{-1} can be attributed

[1]This chapter contains modified part manuscript under preparation by **Billet Romain**, Binglin Zeng, Hongyan Wu, James Lockhart, Mike Gattrell, Hongying Zhao, and Xuehua Zhang. "Effects of Switching Conditions on Switchable Solvent Residue in Polystyrene Microparticles from Emulsion Extraction".

to sulfuric acid, the most abundant compound in the solution. In previous works on the Raman spectroscopy of sulfuric acid solutions [91–93], the 890 cm^{-1} peak was attributed to the asymmetric stretching vibration of HSO_4^-, while the 982 and 1050 cm^{-1} peaks were attributed respectively to the symmetric stretching vibration of HSO_4^- and SO_4^{2-}.

Fig. 4.1(b) shows an enlargement of the peak situated at 778 cm^{-1}, the characteristic peak of extracted DMCHA. The peak at 778 cm^{-1} does not appear without DMCHA while the intensity is correlated with the concentration of DMCHA injected in the toluene solution. Previous work assigned the peaks in the spectral range from 400 to 1600 cm^{-1} in N,N-Dimethylaniline (DMA) to the vibration modes of the ring [94, 95]. As the molecular structure of DMA is similar to that of DMCHA, the characteristic peak at 778 cm^{-1} can be assigned to a vibration mode of the ring in DMCHA.

Fig. 4.1(c) shows the intensity of the peak at 778 cm^{-1} against the concentration of DMCHA in the toluene solution. The intensity of the peak follows a linear relationship with the DMCHA concentration in the range of 0.5 to 2.3 g/L. For as low as 0.4 and 0.3 g/L of DMCHA in toluene, the peak is still detectable. However, the intensity of the characteristic peak deviated from the linear fitting, thus setting the limit of quantification (LOQ) at 0.5 g/L. The residual characteristic peak cannot be distinguished from the noise at 0.15 g/L, so the limit of detection (LOD) is set at 0.3 g/L. In the linear range from 0.5 mg to 2.3 g/L of DMCHA, the intensity of the 778 cm^{-1} after extraction can be used to quantify the residual DMCHA peak by matching the intensity of the characteristic peak to the DMCHA mass through this calibration curve.

To quantify the residue in the PS particles prepared from emulsion extraction, we followed our extraction method to separate the residual solvent from polystyrene. The filtered polystyrene with trapped solvent is washed by an acid solution, dried, and then dissolved in toluene. The aqueous extractant phase is then analyzed using

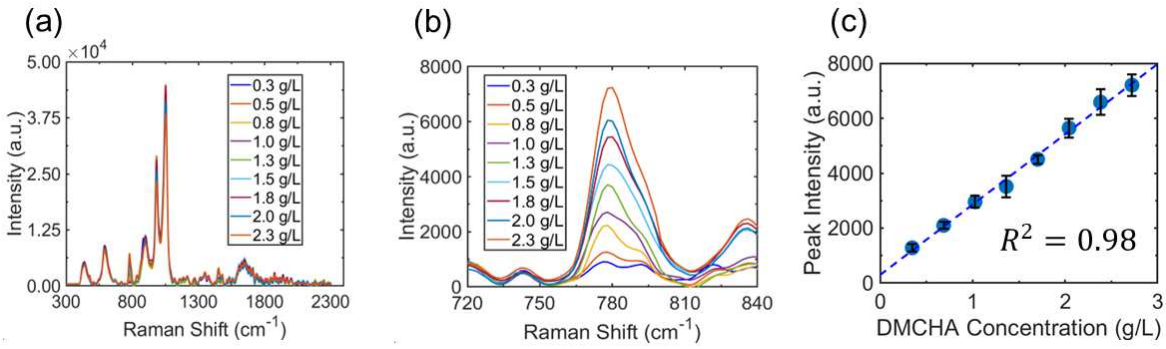

Figure 4.1: (a) Standard Raman spectra of the aqueous phase containing the extracted DMCHA. The concentration of DMCHA ranges from 0.3 to 2.3 g/L in the toluene phase. (b) Characteristic peak of DMCHA around 778 cm^{-1}. An increased concentration of DMCHA in the toluene phase results in an increase of the intensity of the peak. (c) Plot of the measured intensity of the characteristic peak of DMCHA at 778 cm^{-1} with the DMCHA concentration in toluene. The blue dashed line represents the linear fitting of the data. The correlation coefficient $R^2 = 0.98$.

Raman spectroscopy and the residue is quantified using the established calibration curve in Fig. 4.1(c).

4.2 Emulsion and particle size distribution

Fig. 4.2(a) shows the initial emulsion droplet size distribution obtained by using focused beam reflectance measurement (FBRM) before the addition of the trigger. A typical droplet size has been found to be between 5 and 30 μm. After the extraction of the switched SHS from the emulsion, the size of the final polystyrene dispersion dropped to the range of 1 to 20 μm. In addition, the particle count decreased after addition of the trigger, possibly due to drop coalescence during the trigger addition.

Fig. 4.2(b) shows a typical confocal image of a polystyrene powder obtained from emulsion extraction of the SHS after the powder was redispersed in ethanol. The particles appear to be isolated spheres, or aggregates as shown in Fig. 4.2(c). Fig. 4.2(d) shows a zoom on a 4-μm particle while Fig. 4.2(e) presents a zoom on a 5-μm particle cluster consisting of 3 particles. The size of the particles obtained from the image shown in Fig. 4.2(f) ranges from about 2 to 7 μm with a mean diameter of

$4.3 \pm 0.9\ \mu m$. The particle size is consistent with the size distribution measured via FBRM. Large particles were also found from FBRM measurements, possibly due to clusters in the mixture. Fig. 4.2(g) shows a 3D image of the particles, and Fig. 4.2(h) shows a close up on one large particle cluster of 25 μm in length.

In earlier works [59], similar aggregates were found in the latexes resulting from emulsion extraction of an SHS. During the process of switching, an acid is added which partially reacts with the SHS to form a salt. A consequence of the acid addition and salt formation is an increase in the ionic strength of the aqueous medium, that may lead to the compression of the electric double layer thus enhancing the likelihood of aggregation of the hydrophobic particles.

4.3 Influence of the trigger addition rate on the solvent residue

We made a range of experiments to study the influence of the total trigger addition duration on the residual solvent. For this set of experiments, we follow the conditions No. 1 described in Table 2.3.The total volume of the trigger solution added into the emulsion is kept constant, therefore an increase in addition rate resulted in a shorter trigger addition duration. The trigger addition rate changed from 0.1 mL/min to 8 mL/min, resulting in switching duration ranging from 7.5 min to 600 min until completion.

Fig. 4.3(a) shows the reproducibility of the characteristic peak of DMCHA for five Raman measurements on one sample. Fig. 4.3(b) shows the Raman characteristic peak of DMCHA measured in the aqueous phase after extraction for different trigger addition duration. The intensity is normalized by the powder weight to take into account the sample mass effect. The Raman characteristic peak is nearly independent of the total trigger addition duration.

Fig. 4.3(c) shows the DMCHA residue against the total trigger addition duration. Each point represents one sample, and the error bar represents the standard deviation

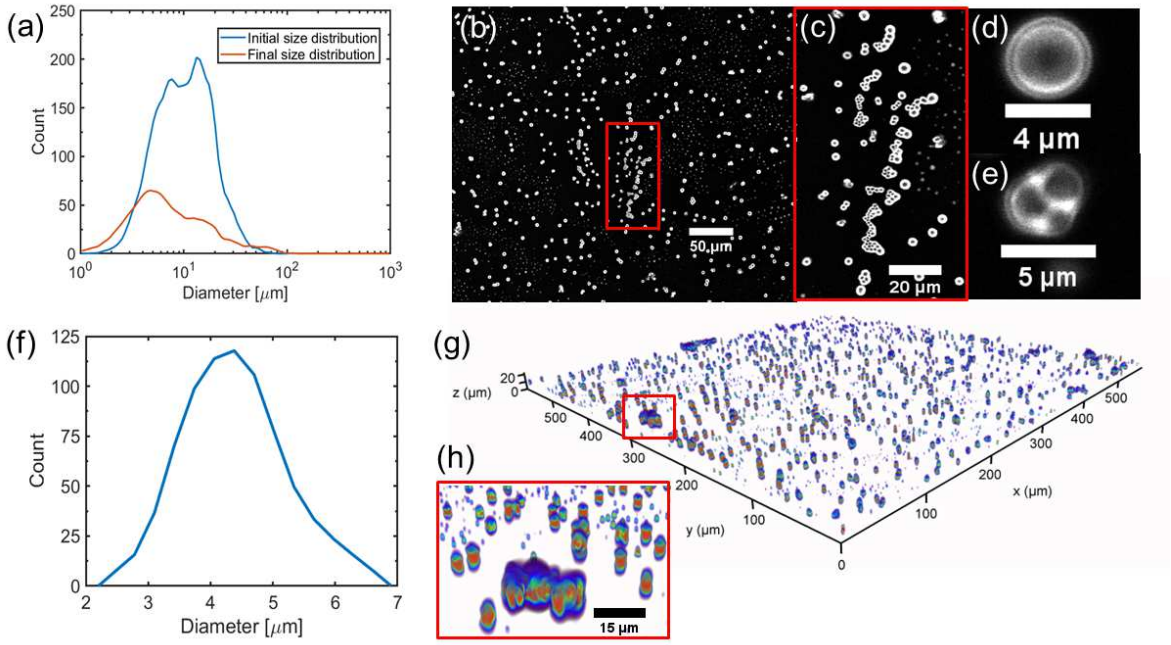

Figure 4.2: (a) Comparison of the size distribution measured via FBRM of the initial emulsion (80:20 wt% aqueous:organic phase ratio at T = 20°C), before trigger addition (2.5 M formic acid solution added in 120 min) and final polystyrene dispersion. (b) Typical confocal microscopy image of a re-dispersed powder resulting from the extraction of SHS from the emulsion. (c) Close-up on aggregated particles inside the powder. (d) Zoom on a single polystyrene particle. (e) Zoom on a particle composed of three smaller particles merged together. (f) Size distribution of the powder shown in (b) measured via image analysis. (g) 3D map of the produced polystyrene powder made by confocal microscopy imaging. (h) Close-up on aggregated particles in the 3D map.

from five Raman spectroscopy measurements. The residual DMCHA found inside of the powder is nearly constant with the trigger addition rate. According to the Raman characteristic peak, the average DMCHA residue found inside of the powder is 7.6 ± 0.6 wt%. This residue is close to what was reported for polystyrene foam recycling using DMCHA in previous work [2].

The driving force for transfer of DMCHA between phases during switching can be described by its distribution coefficient [14]. The distribution coefficient of DMCHA is defined as the ratio between the DMCHA concentration in the organic phase and in the aqueous phase:

$$D = \frac{[DMCHA^0]_{org} + [DMCHAH^+]_{org}}{[DMCHA^0]_{aq} + [DMCHAH^+]_{aq}} \tag{4.1}$$

With $[DMCHA^0]_{org}$ and $[DMCHAH^+]_{org}$ being the concentration in the organic phase of the neutral and protonated forms of DMCHA respectively. Similarly, $[DMCHA^0]_{aq}$ and $[DMCHAH^+]_{aq}$ respectively refer to the concentration in the aqueous phase of the neutral and protonated forms of DMCHA.

In our experiments, DMCHA is in equilibrium between an organic phase, polystyrene, and an aqueous phase, the trigger solution. During the switching of the emulsion, the pH of the aqueous phase steadily decreases. As neutral DMCHA is converted to protonated DMCHA through an acid-base reaction, the distribution coefficient is directly dependent on the pH of the aqueous phase. Fig. 4.3(c) shows the sketch of a distribution coefficient against the pH of the aqueous phase, as it was modeled in previous works [14]. Area (I) corresponds to the high pH region at the beginning of our experiment, where DMCHA is mostly present in the organic phase. At high pH, D can be simplified by the partition coefficient of the neutral form of DMCHA $K = \frac{[DMCHA^0]_{org}}{[DMCHA^0]_{aq}}$ and is therefore constant with pH change. As trigger solution is added, the pH of the aqueous phase starts decreasing and reaches area (II). This region corresponds to the switching of DMCHA from hydrophobic (neutral form) to hydrophilic (protonated form) where DMCHA transfers from the organic phase

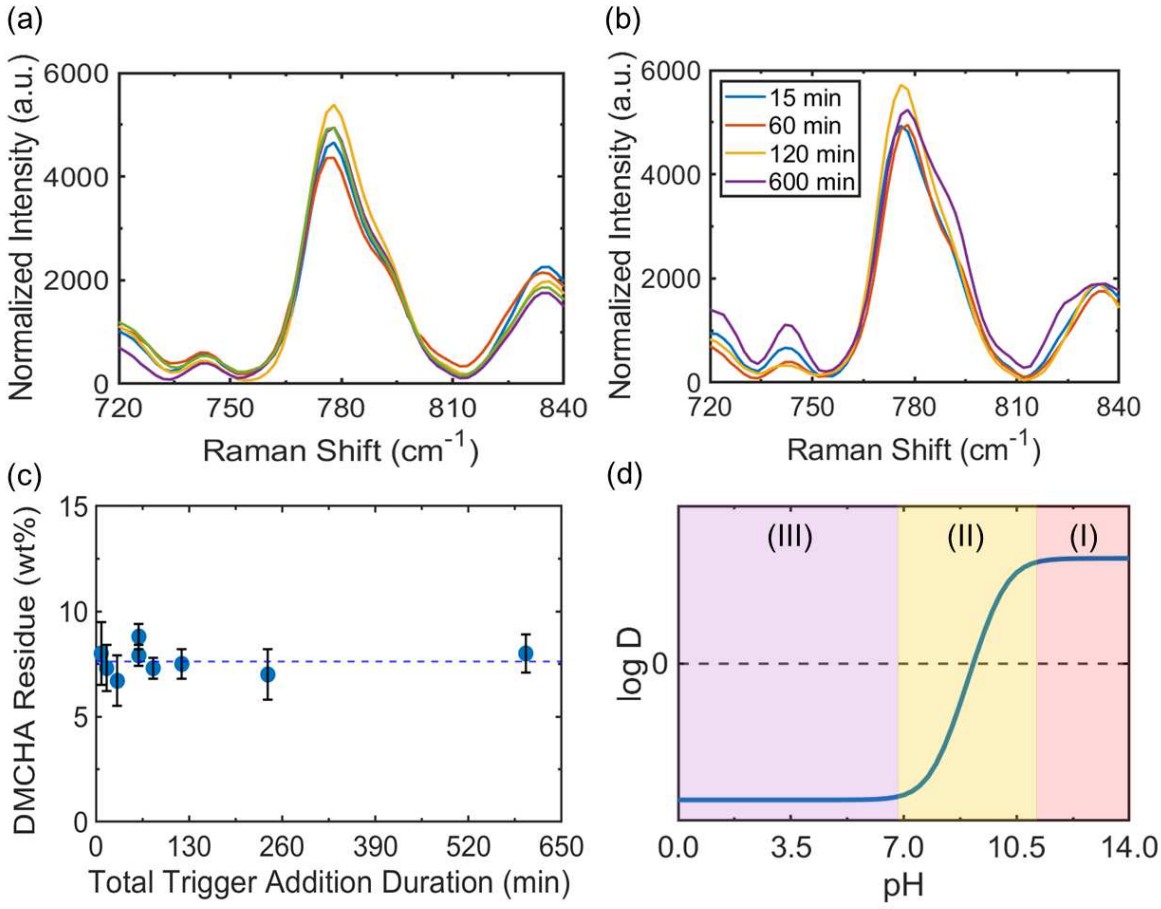

Figure 4.3: (a) The characteristic peak of DMCHA from five measurements after extraction of the sample made with condition No.1 in table 2.3 for a total trigger addition duration of 120 min. (b) DMCHA characteristic peak for powders from different total trigger addition duration (Conditions No.1, table 2.3). (c) Plot of the DMCHA residue against the total trigger addition duration. Each point represents one powder sample. The error bar represents the standard deviation over 5 Raman measurements. A constant DMCHA residue of 7.6 $\pm$ 0.6 wt% is found with varying trigger addition duration. (d) Sketch of the distribution coefficient of an SHS between an organic and aqueous phase against the pH of the aqueous phase. Area (I) corresponds to high pH, before addition of the trigger. Area (II) shows the range of pH characteristic of the switching process where DMCHA starts to be protonated. Area (III) corresponds to the low pH region, where most DMCHA will stay in the aqueous phase.

to the aqueous phase. After switching, the aqueous phase reaches the low pH area (III) where D reaches a plateau. In this region, D can be simplified by the partition coefficient of the protonated form of DMCHA $K' = \frac{[DMCHA^+]_{org}}{[DMCHA^+]_{aq}}$.

The distribution coefficient describes the equilibrium that would occur given sufficient time. However, mass transfer from within the emulsion drop to the organic-aqueous interface can delay the approach to equilibrium. As DMCHA is extracted from the emulsion drop, the PS will begin to precipitate, decreasing the mobility of the remaining DMCHA in the drop. Therefore, the trigger solution addition rate which will affect how fast the emulsion switches might be expected to influence the removal of DMCHA from the emulsion drops and so the residual concentration in the final PS powder. However, withing the ranges tested no significant effect was noted.

4.4 Trigger solution concentration impact on the solvent residue

Another series of experiments was performed to examine the influence of the trigger solution concentration on the DMCHA residue. The conditions No. 2 from table 2.3 were followed. The total volume of the trigger solution added was 60 ml, but the concentration of formic acid in the solution was changed from 2.5 to 5 M.

Fig. 4.4(a) shows the Raman spectra of the aqueous phase resulting of the extraction at different trigger solution concentrations. The intensity is normalized by the mass of the powder sample. Similar to the trigger addition rate, the characteristic peak intensity is weakly dependent on the trigger concentration.

Fig. 4.4(b) present the extrapolated DMCHA residue from the calibration curve. The DMCHA residue is nearly constant with changing formic acid concentration. An average DMCHA residue of 7.5 $\pm$ 0.3 is found inside of the polystyrene powders.

The observed result can also be explained by the distribution coefficient at equilibrium. At low pH, the DMCHA residue after switching is proportional to the distribution coefficient. In the low pH region, the distribution coefficient is constant and equal

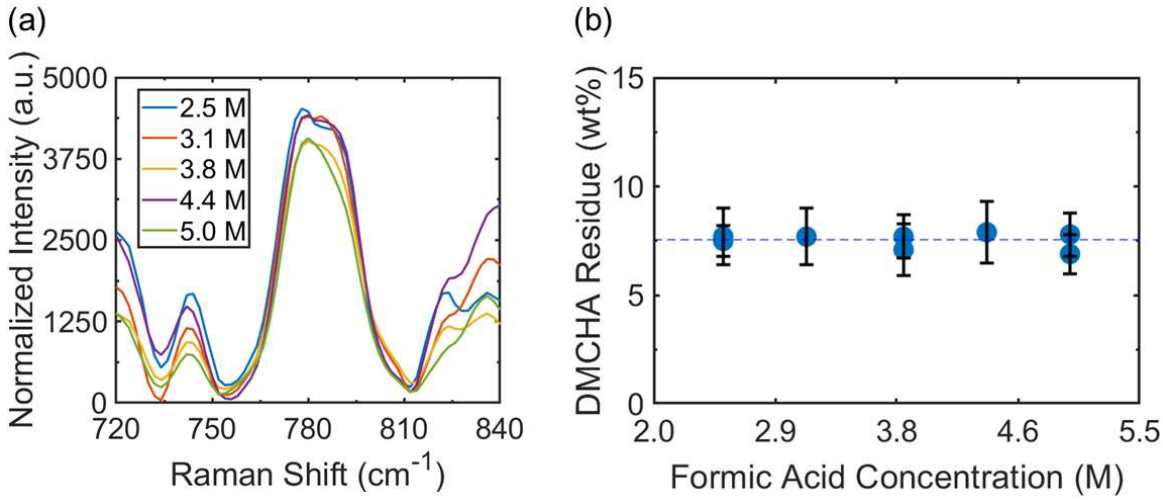

Figure 4.4: (a) DMCHA characteristic peak of the extractant aqueous phase after extraction from the powders samples made with different trigger solution concentration. The organic fraction was kept constant at 20 wt%, while formic acid solutions were used as the trigger and added in 120 min. The temperature was kept at 20°C. (b) Plot of the DMCHA residue against the trigger solution concentration. The error bars represent the standard deviation over five Raman measurements.

to the partition coefficient of the protonated form of DMCHA K'. When increasing the trigger solution concentration, the final pH of the aqueous phase decreases, which does not shift the distribution coefficient, and therefore the level of DMCHA residue in the particles as observed in our experiment.

4.5 Organic phase fraction impact on the solvent residue

The emulsion composition was varied to investigate the change in DMCHA solvent residue inside the resultant powder. The temperature, trigger addition rate, and trigger concentration were all held constant throughout this set of experiments. Fig. 4.5(a) shows the Raman peak at 778 cm^{-1} for powder made from emulsion with different organic phase fractions. Conditions No. 3 were used for this set of experiment. The range of organic phase fraction studied was between 10 to 30 wt%.

In this experiment, the detected Raman characteristic peak depends on the organic

phase fraction used for the emulsion preparation. A smaller organic phase fraction resulted in an increased intensity of the Raman characteristic peak of DMCHA. Fig. 4.5(b) presents the residual DMCHA, which is found to decrease with an increase in the organic phase fraction. At 10 wt% of organic phase fraction, the DMCHA residue in the resulting polystyrene powder was 19.2 ± 1.6 wt%. However, at higher organic phase fraction, the resulting residual solvent in the powder was reduced to 5.7 ± 0.8 wt%. Emulsion with an organic phase fraction lower than 10 wt% and higher than 30 wt% was unstable and no powder was formed. A similar effect of the organic to aqueous phase ratio on the residual solvent has previously been reported for the extraction of bitumen with TEDPA [82].

This effect could be explained by water trapped inside the PS particles, resulting in a small fraction of the solvent remaining as dissolved protonated DMCHA. Fig. 4.5(c) shows the photo of the toluene phase after dissolution of the produced polystyrene. During the polystyrene dissolution, the toluene phase becomes cloudy, and a second minor immiscible water phase can be detected at the bottom of the toluene phase. The presence of the cloudy phase indicates the existence of water microdroplets as an emulsion, that may be stabilised by residual SDS in the powder.

It was observed that when lowering the organic phase content under 20 wt% in the emulsion, some of the polystyrene was recovered as a solid chunk shown in Fig. 4.5(d). Nearly 50 wt% of the polystyrene was recovered as powder while the remaining polystyrene was aggregated in the form of a polystyrene chunk for 10 wt% of organic phase in the emulsion. The higher organic phase fraction would result in a higher final concentration of switched DMCHA in the aqueous phase and one possibility is that this may stabilize the PS particles and inhibit their agglomeration. Fig. 4.5(e) shows the FTIR absorbance spectra of both the polystyrene powder and polystyrene chunk. In both cases, typical water bands due to vibrations of the O-H bond were observed at 3000 - 3500 cm^{-1} and 1500 - 1700 cm^{-1}. However, the magnitudes of the water bands were higher in the polystyrene chunk. More water was therefore

trapped during the polystyrene chunk formation leading to higher DMCHA residue in the recovered polystyrene.

4.6 Influence of emulsion temperature on the solvent residue

The effect of the temperature at which the switching of the emulsion occurs was also studied. Conditions No. 4 in table 2.3 were used. The temperature was kept homogeneous through the use of a water bath paired with constant mixing at 300 RPM. A temperature difference of 0.5°C was observed between the bottom and top of the emulsion.

Fig. 4.6(a) shows the Raman spectra of DMCHA normalized by the sample mass after extraction from the powders for different temperatures. The temperatures studied ranged from 15 °C to 90°C. The normalized intensity of the DMCHA characteristic peak increases with an increase in temperature, suggesting a higher DMCHA residue as the temperature increases. Fig. 4.6(b) shows the DMCHA residue extrapolated from the calibration curve. The DMCHA residue increases from 6.3 wt % at 15°C to 17.8 wt% at 90°C.

An increase in the DMCHA residue had previously been reported during lipid extraction from microalgae [24]. Two reasons can be suggested to explain the increase in residue content at higher temperature. Firstly, the distribution coefficient of DMCHA between polystyrene and water may be affected by the temperature. At low pH, as most of DMCHA is protonated, the distribution coefficient is reduced to the partition coefficient of protonated DMCHA. Higher temperature may improve the solubility of charged DMCHA in the polystyrene phase relatively to the solubility in the aqueous phase. [96, 97]

Secondly, the change in temperature may also increase the partition of water inside of DMCHA, leading to a higher amount of trapped water in the droplet. Fig 4.6(c) shows snapshots of a dissolving 90:10 wt% DMCHA/polystyrene sessile drop inside of

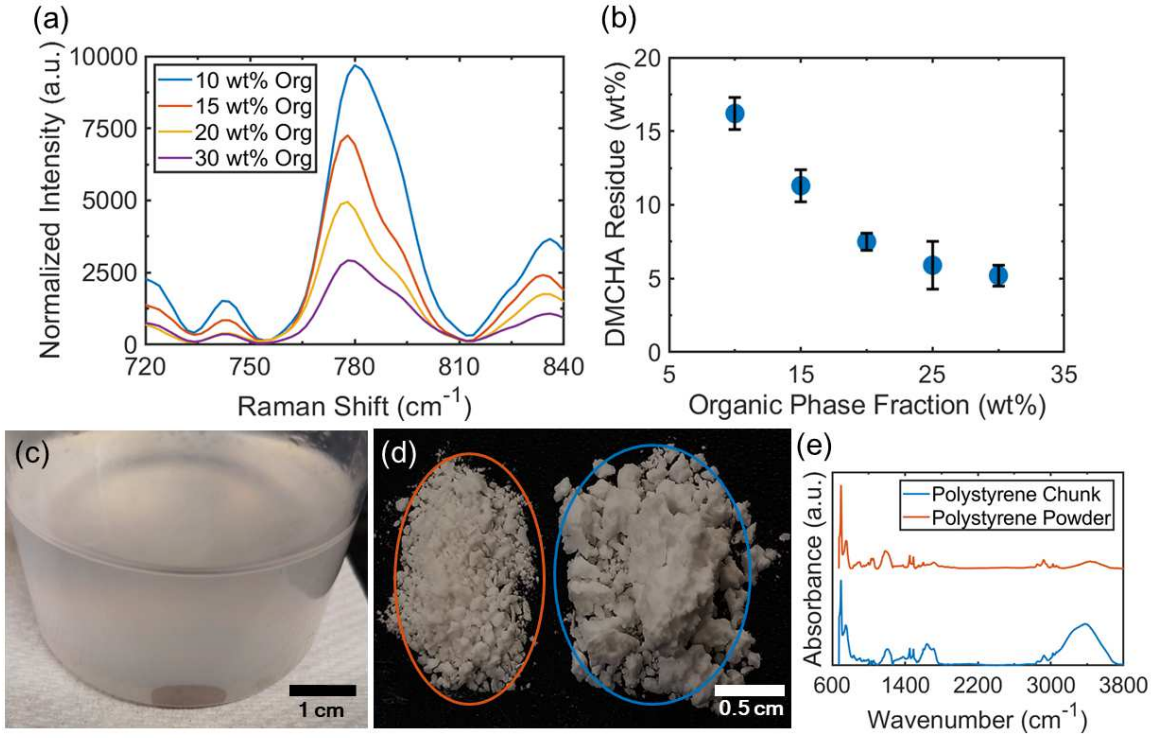

Figure 4.5: (a) DMCHA characteristic peak of the extractant aqueous phase after extraction from the powder made from emulsion with different organic phase fraction. 2.5 M of formic acid solution was used as the trigger, added in 120 min. The temperature of the emulsion was 20°C. (b) Plot of the DMCHA residue against the organic fraction in the emulsion. Each point represent one powder and the error bar represents the standard deviation over five Raman measurements. A decrease in DMCHA residue was found with an increase in the organic fraction in the emulsion. (c) Toluene phase during the extraction process after dissolution of polystyrene. A second water phase appears during the polystyrene dissolution showing that water was trapped in the recovered polystyrene. (d) Recovered polystyrene from a 10 wt% organic phase emulsion switched at 20°C with a 2.5 M formic acid solution. In orange is highlighted the polystyrene recovered in powder form, while the blue area highlights polystyrene recovered as a solid chunk. (e) Corresponding FTIR measurement of the polystyrene powder and chunk. Both samples exhibit the characteristic bands of water, especially inside of the polystyrene chunk.

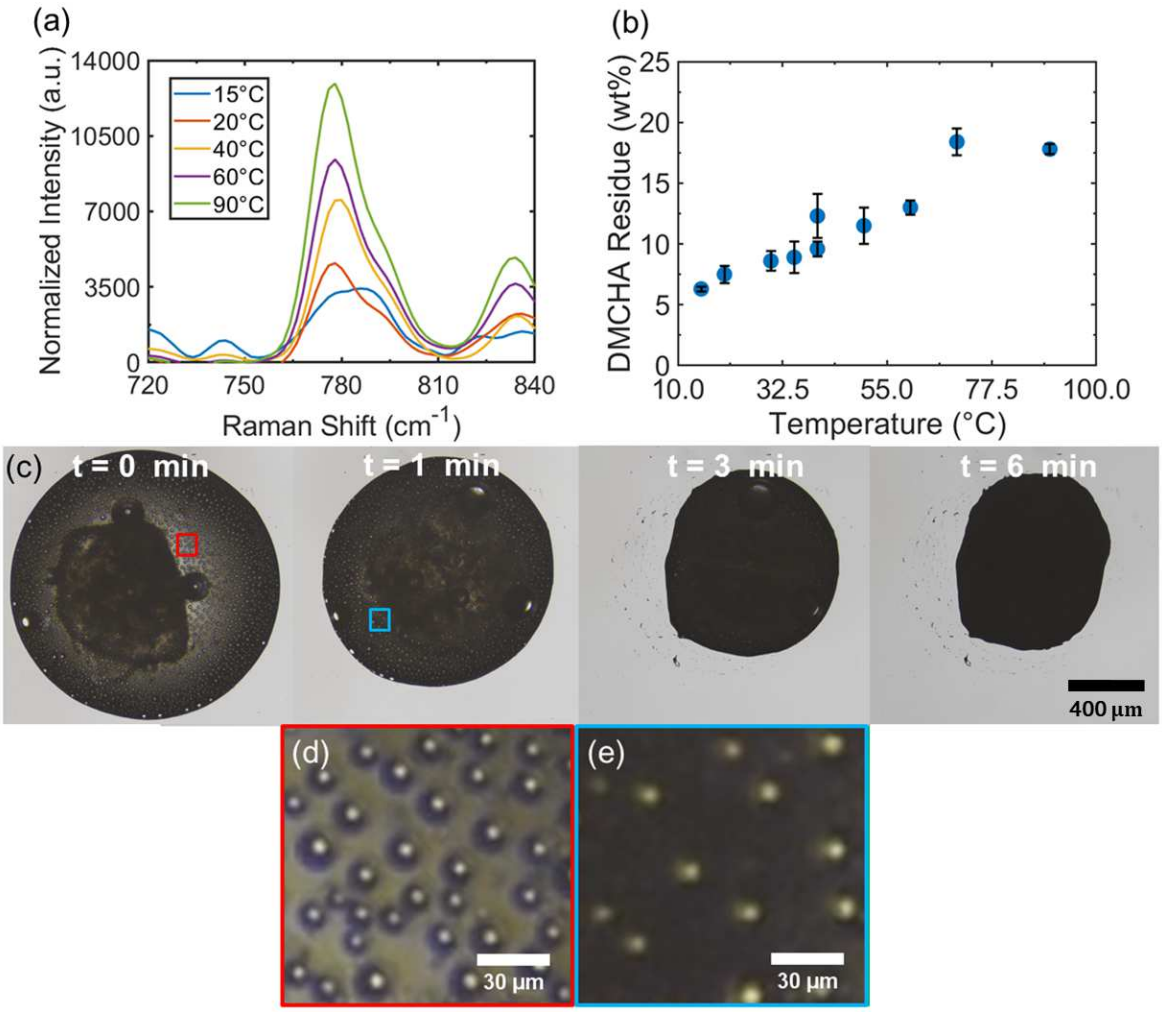

Figure 4.6: (a) DMCHA characteristic peak of the extractant aqueous phase after extraction for powders made at different temperature. The organic fraction was kept constant at 20 wt%. 2.5 M of formic acid solution was used as the trigger, added in 120 min. (b) Plot of the DMCHA residue against the emulsion temperature for different powders. Each point represents one powder and the error bar represents the standard deviation over five Raman measurements. The DMCHA residue is found to increase with the temperature from 6.3 wt% at 15°C to 17.8 wt% at 90 °C. (c) Snapshots of a single sessile 90/10 DMCHA/polystyrene drop in a 0.1 M formic acid solution bath at 90°C observed from an upright optical microscope during the extraction process of the drop. A phase separation behavior is observed with precipitated polystyrene at the center of the drop and water droplets in the DMCHA-rich phase of the drop. At right side is the final polystyrene particle. (d-e) Expanded view of water droplets observed inside the DMCHA/polystyrene drop.

a 0.1 M formic acid trigger bath at a high 90°C temperature. During this experiment, the DMCHA is solubilized by switching similarly to the emulsion extraction process. In this experiment, polystyrene precipitates at the center of the drop, similar to the observed precipitated polystyrene during the emulsion formation. Water droplets are observed moving freely inside of the DMCHA-rich phase. Fig. 4.6(d-e) shows a zoom on some of the water droplets observed. As the drop shrinks, the water droplets follow the movement of the drop boundary. Some water droplets remain trapped in the polystyrene particle after the DMCHA drop dissolution.

This phase separation behavior has been observed at room temperature in previous work [98]. Similarly, water droplets are observed following the shrinking interface of the drop. At the end of the dissolution process, the increase of the viscosity of the drop fixes the water droplets that remain trapped in the particle. However, at high temperature, larger and more water droplets can be observed. Increased trapped water phase in the high temperature case may store more protonated DMCHA, resulting in larger residual solvent in the particles.

4.7 Influence of the trigger type on the solvent residue

We investigate the influence of trigger type on the residual DMCHA in the polystyrene after switching DMCHA from emulsions. The triggers studied are formic acid, sulfuric acid and dry ice. Fig. 4.7(a-c) shows pictures of the recovered polystyrene for each trigger type. For the formic Fig. 4.7(a) and sulfuric acid Fig. 4.7(b) triggers the experiments yields a powder. However, for the dry ice trigger Fig. 4.7(c), the polystyrene is recovered as a single aggregate.

Fig. 4.7(d) shows the DMCHA residue in the recovered polystyrene. Unwashed samples yielded a high DMCHA residue of around 15 wt%, however, it was shown that adding an acidic phase washing step can reduce the DMCHA residue by 4 wt% in the sulfuric acid case to 7.5 wt% for the formic acid trigger. The difference in residue

between washed and unwashed sample can be attributed to the residual DMCHA present on the surface of the recovered polystyrene. The acidic washing solution can solubilize the surface DMCHA during the washing step contributing to a reduction in final residue.

For washed samples, the sulfuric acid trigger yielded polystyrene with 10.3 ± 1.0 wt% residual DMCHA, dry ice yielded polystyrene with 9.2 ± 1.6 wt% DMCHA and the formic acid was able to yield a polystyrene powder with 7.7 ± 1.3 wt% DMCHA. There is a slight influence of the trigger type on the residual DMCHA, however, a Student's t-test showed that only the residual DMCHA between the formic and sulfuric acid trigger was significant. The different cations present during the switching of DMCHA from the emulsion might explain the difference in DMCHA residue between the two triggers. The different cations may influence the distribution coefficient and therefore change the residual DMCHA observed [99]. In previous works on pharmaceutical compounds, the salt has also been found to influence the distribution coefficient [100]. However, this effect is still low in magnitude to the one observed for the temperature and emulsion composition.

4.8 Conclusions

In this work, polystyrene microparticles were prepared by dissolution of SHS from emulsion droplets containing polystyrene and an SHS initially in the hydrophobic state. An acidic aqueous solution was used as the trigger to switch the SHS to the water soluble state. The residual SHS inside of the polystyrene microparticles was quantified by Raman spectroscopy after extraction from dissolved particles. Our results showed that the residual SHS remained constant at 7.6 ± 0.5 wt% of the recovered powder with varying trigger addition rate and trigger concentration. But the SHS residue level changed with trigger types used to switch DMCHA, attributed to the influence o different cations on the distribution coefficient of the SHS in water and in the organic phase.

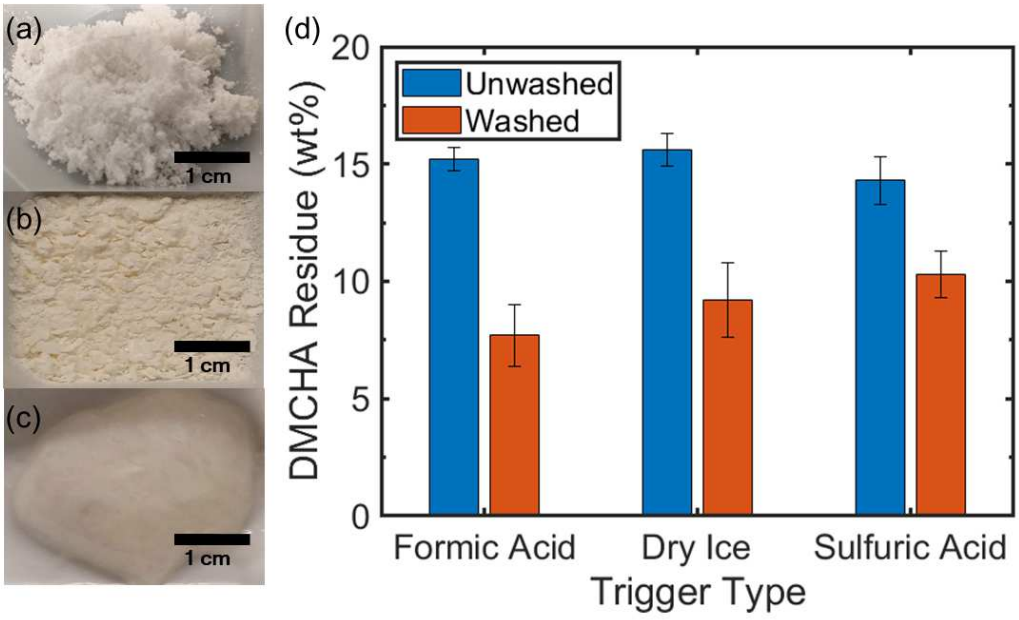

Figure 4.7: Images of the polystyrene recovered with (a) formic acid, (b) sulfuric acid and (c) dry ice. (d) DMCHA residue for formic acid, dry ice and sulfuric acid, with and without the acid washing step by 0.9 M sulfuric acid solution . The error represents the standard deviation over five Raman spectroscopy measurements. The washing step removed DMCHA that was present on the surface of the powders.

Importantly, by decreasing the organic phase fraction from 30 to 10 wt%, the SHS residue was found to increase from 5.2 to 16.2 wt%, while an increase in temperature from 15 to 90 °C also led to an increase in the residual SHS from 6.3 wt% to 17.8 wt%. The higher residue at higher temperature could be attributed to more trapped water inside the recovered polystyrene particles due to increased agglomeration at high temperatures and with low organic phase fraction. The confined water carried the SHS in the water soluble form, leading to a higher SHS residual inside the final product. The correlation between the residue content and water trapped in the emulsion drops is a new mechanism, suggesting that an effective way to reduced solvent residue may be to decrease the water entrapped in the emulsion droplets.

Chapter 5

Conclusions & future work

5.1 Main results and contribution

In chapter 3, we investigated the dynamics and in-drop phase separation during the dissolution process of drops of SHS, water and polymer in a trigger solution. Switching DMCHA to the hydrophilic form at the drop surface led to the dissolution of the drops of DMCHA and polystyrene. An increase in both trigger concentration and initial polystyrene composition decreased the lifetime of the drop. The lifetime of the dissolving drops followed a scaling relationship between the drop lifetime and the initial drop volume. An overall scaling coefficient of 0.53 ± 0.07 was found based on 70 different initial conditions, suggesting that the dissolution rate was in-between the diffusion-dominated and convection driven dissolution. Along with drop dissolution, water intake into the drop led to in-drop precipitation of polystyrene as water acts as a non-solvent for polystyrene. Water microdroplets formed through in-drop nucleation from reduced solubility of water in concentrated drops, and contributed to the porous microstructure of the final polystyrene particle.

In chapter 4, the residual SHS inside of polystyrene microparticles prepared by dissolution of emulsion droplets containing polystyrene and a SHS in the hydrophobic state was studied. The residual SHS inside of the particles was quantified by Raman spectroscopy after extraction from dissolved particles. Our results showed that the residual SHS remained constant at 7.6 ± 0.5 wt% of the recovered powder with varying

trigger addition rate and trigger concentration. But the SHS residue level changed with trigger types used to switch DMCHA, attributed to the influence of different cations on the distribution coefficient of the SHS in water and in the organic phase. By decreasing the organic phase fraction from 30 to 10 wt%, the SHS residue was found to increase from 5.2 to 16.2 wt%, while an increase in temperature from 15 to 90 °C also led to an increase in the residual SHS from 6.3 wt% to 17.8 wt%. The higher residue at higher temperature could be attributed to more trapped water inside the recovered polystyrene particles due to increased agglomeration at high temperatures and with low organic phase fraction. The confined water carried the SHS in the water soluble form, leading to a higher SHS residual inside the final product.

The findings from this thesis may help to give a quantitative understanding of the switching dynamics of SHS drops during the initial external reaction/diffusion dominated phase, and provide useful insights for internal drop dynamics and improved design for SHS switching processes in applications such as latex formation. Moreover, the correlation between the residue content and water trapped in the emulsion drops is a new mechanism, suggesting that an effective way to reduced solvent residue may be to decrease the water entrapped in the emulsion droplets.

5.2 Future work

The work in this thesis focused on the switching dynamics of SHS/polymer drops and on the residual solvent left inside of the particles which are two fundamental issues related to the applications of SHSs. There are several aspects of this work that could be interesting to focus on and to improve our understanding of the phenomenon in future:

1. The effect on the drop dissolution dynamics of different types of SHSs. While in this thesis we studied the effect of the trigger concentration and drop composition, the effects of the types of SHSs have not been explored. This is an

interesting point of study as the SHS is the main component of the switching-induced drop dissolution. Further understanding the role of the SHS molecular structure on the dissolution dynamics may help develop better SHSs with faster dissolution times.

2. Similarly, the effect of the polymer on the drop dissolution dynamics can also be an interesting point to study. In our study, we only focused on polystyrene, the exact role of the polymer on the drop dissolution is still unclear. Using other polymers may allow a finer control of the dissolution dynamics and help design particles with desired structures.

3. While our work showed the phase separation behavior observed in the SHS/polymer drop, and related the trapped water phase with the residual solvent, we were not able to find a way to decrease the trapped water phase. Future works based on removing the trapped water phase may allow to reduce the residual solvent inside of the particles.

4. On another hand, the nucleation of water droplets may benefit some applications. For instance, the mechanism of the phase separation is actively used in other domains such as the production of porous membranes via phase inversion. SHSs could prove beneficial for applications requiring a phase separation during the solvent removal step.

Bibliography

[1] P. G. Jessop, L. Phan, A. Carrier, S. Robinson, C. J. Dürr, and J. R. Harjani, "A solvent having switchable hydrophilicity," *Green Chemistry*, vol. 12, no. 5, pp. 809–814, 2010.

[2] P. G. Jessop *et al.*, "Tertiary amine solvents having switchable hydrophilicity," *Green Chemistry*, vol. 13, no. 3, pp. 619–623, 2011.

[3] E. Yilmaz and M. Soylak, "Switchable polarity solvent for liquid phase microextraction of cd (ii) as pyrrolidinedithiocarbamate chelates from environmental samples," *Analytica chimica acta*, vol. 886, pp. 75–82, 2015.

[4] G. Lasarte-Aragonés, R. Lucena, S. Cárdenas, and M. Valcárcel, "Use of switchable solvents in the microextraction context," *Talanta*, vol. 131, pp. 645–649, 2015.

[5] M Ezoddin, K Abdi, and N Lamei, "Development of air assisted liquid phase microextraction based on switchable-hydrophilicity solvent for the determination of palladium in environmental samples," *Talanta*, vol. 153, pp. 247–252, 2016.

[6] A. G. Moghadam, M. Rajabi, M. Hemmati, and A. Asghari, "Development of effervescence-assisted liquid phase microextraction based on fatty acid for determination of silver and cobalt ions using micro-sampling flame atomic absorption spectrometry," *Journal of Molecular Liquids*, vol. 242, pp. 1176–1183, 2017.

[7] C. Vakh, A. Pochivalov, V. Andruch, L. Moskvin, and A. Bulatov, "A fully automated effervescence-assisted switchable solvent-based liquid phase microextraction procedure: Liquid chromatographic determination of ofloxacin in human urine samples," *Analytica Chimica Acta*, vol. 907, pp. 54–59, 2016.

[8] S. Shahraki, H. Ahmar, and M. Nejati-Yazdinejad, "Electrochemical determination of nitrazepam by switchable solvent based liquid-liquid microextraction combined with differential pulse voltammetry," *Microchemical Journal*, vol. 142, pp. 229–235, 2018.

[9] A. L. Oenning, L. Birk, S. Eller, T. F. de Oliveira, J. Merib, and E. Carasek, "A green and low-cost method employing switchable hydrophilicity solvent for the simultaneous determination of antidepressants in human urine by gas chromatography-mass spectrometry detection," *Journal of Chromatography B*, vol. 1143, p. 122 069, 2020.

[10] M. Behpour, S. Nojavan, S. Asadi, and A. Shokri, "Combination of gel - electromembrane extraction with switchable hydrophilicity solvent-based homogeneous liquid-liquid microextraction followed by gas chromatography for the extraction and determination of antidepressants in human serum, breast milk and wastewater," *Journal of Chromatography A*, vol. 1621, p. 461 041, 2020.

[11] S. K. Shahvandi, M. H. Banitaba, and H. Ahmar, "Development of a new ph assisted homogeneous liquid-liquid microextraction by a solvent with switchable hydrophilicity: Application for gc-ms determination of methamphetamine," *Talanta*, vol. 184, pp. 103–108, 2018.

[12] J. R. Vanderveen, J. Durelle, and P. G. Jessop, "Design and evaluation of switchable-hydrophilicity solvents," *Green Chemistry*, vol. 16, no. 3, pp. 1187–1197, 2014.

[13] J. Durelle, J. R. Vanderveen, Y. Quan, C. B. Chalifoux, J. E. Kostin, and P. G. Jessop, "Extending the range of switchable-hydrophilicity solvents," *Physical Chemistry Chemical Physics*, vol. 17, no. 7, pp. 5308–5313, 2015.

[14] J. Durelle, J. R. Vanderveen, and P. G. Jessop, "Modelling the behaviour of switchable-hydrophilicity solvents," *Physical Chemistry Chemical Physics*, vol. 16, no. 11, pp. 5270–5275, 2014.

[15] J. R. Vanderveen, J. Geng, S. Zhang, and P. G. Jessop, "Diamines as switchable-hydrophilicity solvents with improved phase behaviour," *RSC advances*, vol. 8, no. 48, pp. 27 318–27 325, 2018.

[16] I. T. Cunha *et al.*, "Amine-free co 2-switchable hydrophilicity solvents and their application in extractions and polymer recycling," *Green Chemistry*, vol. 24, no. 9, pp. 3704–3716, 2022.

[17] A. J. Haagen-Smit, "Chemistry and physiology of los angeles smog," *Industrial & Engineering Chemistry*, vol. 44, no. 6, pp. 1342–1346, 1952.

[18] R. Atkinson and J. Arey, "Atmospheric degradation of volatile organic compounds," *Chemical reviews*, vol. 103, no. 12, pp. 4605–4638, 2003.

[19] M. Poliakoff, J. M. Fitzpatrick, T. R. Farren, and P. T. Anastas, "Green chemistry: Science and politics of change," *Science*, vol. 297, no. 5582, pp. 807–810, 2002.

[20] F. M. Kerton and R. Marriott, *Alternative solvents for green chemistry*. Royal Society of chemistry, 2013.

[21] A. Holland, D. Wechsler, A. Patel, B. M. Molloy, A. R. Boyd, and P. G. Jessop, "Separation of bitumen from oil sands using a switchable hydrophilicity solvent," *Canadian Journal of Chemistry*, vol. 90, no. 10, pp. 805–810, 2012.

[22] L. Phan, H. Brown, J. White, A. Hodgson, and P. G. Jessop, "Soybean oil extraction and separation using switchable or expanded solvents," *Green chemistry*, vol. 11, no. 1, pp. 53–59, 2009.

[23] K. J. Viner, H. M. Roy, R. Lee, O. He, P. Champagne, and P. G. Jessop, "Transesterification of soybean oil using a switchable-hydrophilicity solvent, 2-(dibutylamino) ethanol," *Green Chemistry*, vol. 21, no. 17, pp. 4786–4791, 2019.

[24] A. R. Boyd, P. Champagne, P. J. McGinn, K. M. MacDougall, J. E. Melanson, and P. G. Jessop, "Switchable hydrophilicity solvents for lipid extraction from microalgae for biofuel production," *Bioresource Technology*, vol. 118, pp. 628–632, 2012.

[25] C. Samorì, L. Pezzolesi, D. L. Barreiro, P. Galletti, A. Pasteris, and E. Tagliavini, "Synthesis of new polyethoxylated tertiary amines and their use as switchable hydrophilicity solvents," *RSC Advances*, vol. 4, no. 12, pp. 5999–6008, 2014.

[26] Y. Du, B. Schuur, S. R. Kersten, and D. W. Brilman, "Opportunities for switchable solvents for lipid extraction from wet algal biomass: An energy evaluation," *Algal research*, vol. 11, pp. 271–283, 2015.

[27] W.-C. Huang, H. Liu, W. Sun, C. Xue, and X. Mao, "Effective astaxanthin extraction from wet haematococcus pluvialis using switchable hydrophilicity solvents," *ACS Sustainable Chemistry & Engineering*, vol. 6, no. 2, pp. 1560–1563, 2018.

[28] H. Liu, W.-C. Huang, N. Guo, and X. Mao, "Application of secondary amine switchable hydrophilicity solvents for astaxanthin extraction from wet haematococcus pluvialis," *Algal research*, vol. 48, p. 101 892, 2020.

[29] D. Fu, S. Farag, J. Chaouki, and P. G. Jessop, "Extraction of phenols from lignin microwave-pyrolysis oil using a switchable hydrophilicity solvent," *Bioresource technology*, vol. 154, pp. 101–108, 2014.

[30] M. H. Tahir *et al.*, "Selective catalytic conversion of tea waste biomass into phenolic-rich bio-oil and subsequent extraction," *Journal of Analytical and Applied Pyrolysis*, vol. 159, p. 105 315, 2021.

[31] L. Wang, Y. Liu, H. Lu, and Z. Huang, "Recycling of phosphorus-containing plastic based on the dual effects of switchable hydrophilicity solvents," *Chemosphere*, vol. 259, p. 127 402, 2020.

[32] C. Samorì *et al.*, "Application of switchable hydrophilicity solvents for recycling multilayer packaging materials," *Green Chemistry*, vol. 19, no. 7, pp. 1714–1720, 2017.

[33] T. Mumladze *et al.*, "Sustainable approach to recycling of multilayer flexible packaging using switchable hydrophilicity solvents," *Green Chemistry*, vol. 20, no. 15, pp. 3604–3618, 2018.

[34] S. Yousef *et al.*, "Cleaner and profitable industrial technology for full recovery of metallic and non-metallic fraction of waste pharmaceutical blisters using switchable hydrophilicity solvents," *Journal of Cleaner Production*, vol. 197, pp. 379–392, 2018.

[35] M. Rezaee, Y. Yamini, and M. Faraji, "Evolution of dispersive liquid–liquid microextraction method," *Journal of Chromatography A*, vol. 1217, no. 16, pp. 2342–2357, 2010.

[36] A. Zgoła-Grześkowiak and T. Grześkowiak, "Dispersive liquid-liquid microextraction," *TrAC Trends in Analytical Chemistry*, vol. 30, no. 9, pp. 1382–1399, 2011.

[37] U. Alshana, M. Hassan, M. Al-Nidawi, E. Yilmaz, and M. Soylak, "Switchable-hydrophilicity solvent liquid-liquid microextraction," *TrAC Trends in Analytical Chemistry*, vol. 131, p. 116 025, 2020.

[38] Y. Bazel, M. Rečlo, and Y. Chubirka, "Switchable hydrophilicity solvents in analytical chemistry. five years of achievements," *Microchemical Journal*, vol. 157, p. 105 115, 2020.

[39] M. Khan and M. Soylak, "Switchable solvent based liquid phase microextraction of mercury from environmental samples: A green aspect," *Rsc Advances*, vol. 6, no. 30, pp. 24 968–24 975, 2016.

[40] S. Zhang, B. Chen, M. He, and B. Hu, "Switchable solvent based liquid phase microextraction of trace lead and cadmium from environmental and biological samples prior to graphite furnace atomic absorption spectrometry detection," *Microchemical Journal*, vol. 139, pp. 380–385, 2018.

[41] Y Bazel, M Reclo, and J Šandrejová, "Using a switchable-hydrophilicity solvent for the extraction- spectrophotometric determination of nickel," *Journal of Analytical Chemistry*, vol. 72, no. 10, pp. 1018–1023, 2017.

[42] C. Yan *et al.*, "Switchable hydrophilicity solvent-based preconcentration for icp-oes determination of trace lead in environmental samples," *Microchemical Journal*, vol. 168, p. 106 529, 2021.

[43] A. Pochivalov, C. Vakh, S. Garmonov, L. Moskvin, and A. Bulatov, "An automated in-syringe switchable hydrophilicity solvent-based microextraction," *Talanta*, vol. 209, p. 120 587, 2020.

[44] H. Ahmar, M. Nejati-Yazdinejad, M. Najafi, and K. S. Hasheminasab, "Switchable hydrophilicity solvent-based homogenous liquid–liquid microextraction (shs-hllme) combined with gc-fid for the quantification of methadone and tramadol," *Chromatographia*, vol. 81, no. 7, pp. 1063–1070, 2018.

[45] D. S. Chormey, S. Bodur, D. Baskın, M. Fırat, and S. Bakırdere, "Accurate and sensitive determination of selected hormones, endocrine disruptors, and pesticides by gas chromatography–mass spectrometry after the multivariate optimization of switchable solvent liquid-phase microextraction," *Journal of separation science*, vol. 41, no. 14, pp. 2895–2902, 2018.

[46] S. Erarpat, A. Cağlak, S. Bodur, S. D. Chormey, Ö. G. Engin, and S. Bakırdere, "Simultaneous determination of fluoxetine, estrone, pesticides, and endocrine disruptors in wastewater by gas chromatography–mass spectrometry (gc–ms) following switchable solvent–liquid phase microextraction (ss–lpme)," *Analytical Letters*, vol. 52, no. 5, pp. 869–878, 2019.

[47] B. Y. Durak, D. S. Chormey, M. Firat, and S. Bakirdere, "Validation of ultrasonic-assisted switchable solvent liquid phase microextraction for trace determination of hormones and organochlorine pesticides by gc–ms and combination with quechers," *Food chemistry*, vol. 305, p. 125 487, 2020.

[48] E. Yip and P. Cacioli, "The manufacture of gloves from natural rubber latex," *Journal of allergy and clinical immunology*, vol. 110, no. 2, S3–S14, 2002.

[49] K. D. Weiss, "Paint and coatings: A mature industry in transition," *Progress in polymer science*, vol. 22, no. 2, pp. 203–245, 1997.

[50] M. A. Winnik, "Latex film formation," *Current opinion in colloid & interface science*, vol. 2, no. 2, pp. 192–199, 1997.

[51] K. Nawamawat, J. T. Sakdapipanich, C. C. Ho, Y. Ma, J. Song, and J. G. Vancso, "Surface nanostructure of hevea brasiliensis natural rubber latex particles," *Colloids and Surfaces A: Physicochemical and Engineering Aspects*, vol. 390, no. 1-3, pp. 157–166, 2011.

[52] Q. Wang, S. Fu, and T. Yu, "Emulsion polymerization," *Progress in polymer science*, vol. 19, no. 4, pp. 703–753, 1994.

[53] W. V. Smith and R. H. Ewart, "Kinetics of emulsion polymerization," *The journal of chemical physics*, vol. 16, no. 6, pp. 592–599, 1948.

[54] K. Lee *et al.*, "Microdroplet-mediated radical polymerization," *ACS Central Science*, 2022.

[55] J. W. Vanderhoff, M. El-Aasser, and J Ugelstad, "Polymer emulsification process," *US patent*, vol. 4, no. 177, p. 177, 1979.

[56] D. Quintanar-Guerrero, E. Allémann, H Fessi, and E. Doelker, "Pseudolatex preparation using a novel emulsion–diffusion process involving direct displacement of partially water-miscible solvents by distillation," *International journal of pharmaceutics*, vol. 188, no. 2, pp. 155–164, 1999.

[57] N Mohammadi, K. Kim, L. Sperling, and A Klein, "Direct miniemulsification of anionically synthesized polystyrene to form uniform submicrometer particles," *Journal of colloid and interface science*, vol. 157, no. 1, pp. 124–130, 1993.

[58] Y.-C. Chen, V. L. Dimonie, O. L. Shaffer, and M. S. El-Aasser, "Development of morphology in latex particles: The interplay between thermodynamic and kinetic parameters," *Polymer international*, vol. 30, no. 2, pp. 185–194, 1993.

[59] X. Su, P. G. Jessop, and M. F. Cunningham, "Preparing artificial latexes using a switchable hydrophilicity solvent," *Green Chemistry*, vol. 19, no. 8, pp. 1889–1894, 2017.

[60] P. S. Epstein and M. S. Plesset, "On the stability of gas bubbles in liquid-gas solutions," *The Journal of Chemical Physics*, vol. 18, no. 11, pp. 1505–1509, 1950.

[61] P. B. Duncan and D. Needham, "Microdroplet dissolution into a second-phase solvent using a micropipet technique: Test of the epstein- plesset model for an aniline- water system," *Langmuir*, vol. 22, no. 9, pp. 4190–4197, 2006.

[62] Y. O. Popov, "Evaporative deposition patterns: Spatial dimensions of the deposit," *Physical Review E*, vol. 71, no. 3, p. 036 313, 2005.

[63] X. Zhang *et al.*, "Mixed mode of dissolving immersed nanodroplets at a solid–water interface," *Soft Matter*, vol. 11, no. 10, pp. 1889–1900, 2015.

[64] R. Picknett and R Bexon, "The evaporation of sessile or pendant drops in still air," *Journal of colloid and Interface Science*, vol. 61, no. 2, pp. 336–350, 1977.

[65] L. Bao *et al.*, "Flow-induced dissolution of femtoliter surface droplet arrays," *Lab on a Chip*, vol. 18, no. 7, pp. 1066–1074, 2018.

[66] Q. Xie and J. Harting, "The effect of the liquid layer thickness on the dissolution of immersed surface droplets," *Soft matter*, vol. 15, no. 32, pp. 6461–6468, 2019.

[67] E. Dietrich, E. S. Kooij, X. Zhang, H. J. Zandvliet, and D. Lohse, "Stick-jump mode in surface droplet dissolution," *Langmuir*, vol. 31, no. 16, pp. 4696–4703, 2015.

[68] E. Dietrich *et al.*, "Role of natural convection in the dissolution of sessile droplets," *Journal of fluid mechanics*, vol. 794, pp. 45–67, 2016.

[69] S. Chu and A. Prosperetti, "Dissolution and growth of a multicomponent drop in an immiscible liquid," *Journal of fluid mechanics*, vol. 798, pp. 787–811, 2016.

[70] E. Dietrich, M. Rump, P. Lv, E. S. Kooij, H. J. Zandvliet, and D. Lohse, "Segregation in dissolving binary-component sessile droplets," *Journal of fluid mechanics*, vol. 812, pp. 349–369, 2017.

[71] H. Tan *et al.*, "Microdroplet nucleation by dissolution of a multicomponent drop in a host liquid," *Journal of fluid mechanics*, vol. 870, pp. 217–246, 2019.

[72] Z. Lu, A. Rezk, F. Jativa, L. Yeo, and X. Zhang, "Dissolution dynamics of a suspension droplet in a binary solution for controlled nanoparticle assembly," *Nanoscale*, vol. 9, no. 36, pp. 13 441–13 448, 2017.

[73] F. Jativa, C. Schütz, L. Bergström, X. Zhang, and B. Wicklein, "Confined self-assembly of cellulose nanocrystals in a shrinking droplet," *Soft Matter*, vol. 11, no. 26, pp. 5374–5380, 2015.

[74] H. Yang *et al.*, "Assembling of graphene oxide in an isolated dissolving droplet," *Soft Matter*, vol. 8, no. 44, pp. 11 249–11 254, 2012.

[75] H. Yang *et al.*, "Tailoring graphene oxide assemblies by pinning on the contact line of a dissolving microdroplet," *Soft matter*, vol. 11, no. 43, pp. 8479–8483, 2015.

[76] W. Sharratt, A Brooker, E. Robles, and J. Cabral, "Microfluidic solvent extraction of poly (vinyl alcohol) droplets: Effect of polymer structure on particle and capsule formation," *Soft Matter*, vol. 14, no. 22, pp. 4453–4463, 2018.

[77] C. E. Udoh, V. Garbin, and J. T. Cabral, "Polymer nanocomposite capsules formed by droplet extraction: Spontaneous stratification and tailored dissolution," *Soft Matter*, vol. 15, no. 26, pp. 5287–5295, 2019.

[78] T. Watanabe, C. G. Lopez, J. F. Douglas, T. Ono, and J. T. Cabral, "Microfluidic approach to the formation of internally porous polymer particles by solvent extraction," *Langmuir*, vol. 30, no. 9, pp. 2470–2479, 2014.

[79] F. Jativa and X. Zhang, "Transparent silk fibroin microspheres from controlled droplet dissolution in a binary solution," *Langmuir*, vol. 33, no. 31, pp. 7780–7787, 2017.

[80] S. Han, K. Raghuvanshi, and M. Abolhasani, "Accelerated material-efficient investigation of switchable hydrophilicity solvents for energy-efficient solvent recovery," *ACS Sustainable Chemistry & Engineering*, vol. 8, no. 8, pp. 3347–3356, 2020.

[81] S. Han *et al.*, "Intensified continuous extraction of switchable hydrophilicity solvents triggered by carbon dioxide," *Green Chemistry*, vol. 23, no. 8, pp. 2900–2906, 2021.

[82] Y. Yang, H. Sui, J. Ma, L. He, and X. Li, "Revealing the residual mechanism of switchable solvents in heavy oil," *Fuel Processing Technology*, vol. 218, p. 106 857, 2021.

[83] R. M. Stephenson, "Mutual solubilities: Water+ cyclic amines, water+ alkanolamines, and water+ polyamines," *Journal of Chemical and Engineering Data*, vol. 38, no. 4, pp. 634–637, 1993.

[84] J. Crolet and M. Bonis, "Ph measurements in aqueous co2 solutions under high pressure and temperature," *Corrosion*, vol. 39, no. 2, pp. 39–46, 1983.

[85] C. Peng, J. P. Crawshaw, G. C. Maitland, J. M. Trusler, and D. Vega-Maza, "The ph of co2-saturated water at temperatures between 308 k and 423 k at pressures up to 15 mpa," *The Journal of Supercritical Fluids*, vol. 82, pp. 129–137, 2013.

[86] S. Wang, C. Zheng, J. Zhao, X. Li, and H. Lu, "Extracting and recovering diesel from oil-based drill cuttings using switchable hydrophilic solvents," *Chemical Engineering Research and Design*, vol. 128, pp. 27–36, 2017.

[87] P. G. De Gennes, "Solvent evaporation of spin cast films:"crust" effects," *The European Physical Journal E*, vol. 7, no. 1, pp. 31–34, 2002.

[88] T. Okuzono, K. Ozawa, and M. Doi, "Simple model of skin formation caused by solvent evaporation in polymer solutions," *Physical review letters*, vol. 97, no. 13, p. 136 103, 2006.

[89] R. D. Deegan, O. Bakajin, T. F. Dupont, G. Huber, S. R. Nagel, and T. A. Witten, "Capillary flow as the cause of ring stains from dried liquid drops," *Nature*, vol. 389, no. 6653, pp. 827–829, 1997.

[90] V. Poulichet, M. Morel, S. Rudiuk, and D. Baigl, "Liquid-liquid coffee-ring effect," *Journal of colloid and interface science*, vol. 573, pp. 370–375, 2020.

[91] D. E. Irish and H Chen, "Equilibriums and proton transfer in the bisulfate-sulfate system," *The Journal of Physical Chemistry*, vol. 74, no. 21, pp. 3796–3801, 1970.

[92] D. Irish and H Chen, "Raman spectral study of bisulfate-sulfate systems. ii. constitution, equilibriums, and ultrafast proton transfer in sulfuric acid," *The Journal of Physical Chemistry*, vol. 75, no. 17, pp. 2672–2681, 1971.

[93] K. Tomikawa and H. Kanno, "Raman study of sulfuric acid at low temperatures," *The Journal of Physical Chemistry A*, vol. 102, no. 30, pp. 6082–6088, 1998.

[94] O Poizat, V Guichard, and G Buntinx, "Vibrational studies of reactive intermediates of aromatic amines. iv. radical cation time-resolved resonance raman investigation of n, n-dimethylaniline and n, n-diethylaniline derivatives," *The Journal of chemical physics*, vol. 90, no. 9, pp. 4697–4703, 1989.

[95] R. A. Ando, D. R. Matazo, and P. S. Santos, "Detailed analysis of the charge transfer complex n, n-dimethylaniline–so2 by raman spectroscopy and density functional theory calculations," *Journal of Raman Spectroscopy*, vol. 41, no. 7, pp. 771–775, 2010.

[96] T. Ingram, T. Mehling, and I. Smirnova, "Partition coefficients of ionizable solutes in aqueous micellar two-phase systems," *Chemical engineering journal*, vol. 218, pp. 204–213, 2013.

[97] D. C. Greminger, G. P. Burns, S. Lynn, D. N. Hanson, and C. J. King, "Solvent extraction of phenols from water," *Industrial & Engineering Chemistry Process Design and Development*, vol. 21, no. 1, pp. 51–54, 1982.

[98] R. Billet, B. Zeng, J. Lockhart, M. Gattrell, H. Zhao, and X. Zhang, "Dissolution dynamics of a binary switchable hydrophilicty solvent - polymer drop into an acidic aqueous phase," *Soft Matter*, pp. –, 2022. DOI: 10.1039/D2SM01275H. [Online]. Available: http://dx.dqi.org/10.1039/D2SM01275H.

[99] C.-S. Chen and S.-T. Lin, "Prediction of ph effect on the octanol–water partition coefficient of ionizable pharmaceuticals," *Industrial & Engineering Chemistry Research*, vol. 55, no. 34, pp. 9284–9294, 2016.

[100] T. Ingram, U. Richter, T. Mehling, and I. Smirnova, "Modelling of ph dependent n-octanol/water partition coefficients of ionizable pharmaceuticals," *Fluid phase equilibria*, vol. 305, no. 2, pp. 197–203, 2011.